Neuro
endocrinology

DOI: 10.1159/000508375
Received: 10/2/2019
Accepted: 5/1/2020
Published(online): 5/4/2020

A novel SEMA3G mutation in two siblings affected by syndromic GnRH deficiency.
Oleari R. André V. Lettieri A. Tahir S. Roth L. Paganoni A. Eberini I. Parravicini C. Scagliotti V. Cotellessa L. Bedogni F. De Martini L.B. Corridori M.V. Gulli S. Augustin H. G. Gaston-Massuet C. Hussain K. Cariboni A.

ISSN: 0028-3835 (Print), eISSN: 1423-0194 (Online)
https://www.karger.com/NEN
Neuroendocrinology

Neuroendocrinology

Manuscript:	NEN-2019-10-5/R2 RESUBMISSION
Title:	A novel SEMA3G mutation in two siblings affected by syndromic GnRH deficiency.
Authors(s):	Roberto Oleari (Co-author), Valentina Andrè (Co-author), Antonella Lettieri (Co-author), Sophia Tahir (Co-author), Lise Roth (Co-author), Alyssa Paganoni (Co-author), Ivano Eberini (Co-author), Chiara Parravicini (Co-author), Valeria Scagliotti (Co-author), Ludovica Cotellessa (Co-author), Francesco Bedogni (Co-author), Lisa Benedetta De Martini (Co-author), Maria Vittoria Corridori (Co-author), Simona Gulli (Co-author), Hellmut G Augustin (Co-author), Carles Gaston-Massuet (Co-author), Khalid Hussain (Corresponding author), Anna Cariboni (Corresponding Author)
Keywords:	Development, Genetics, Gonadotropin-releasing hormone, Immunohistochemistry, Plexins, Puberty, Reproduction, Semaphorins
Type:	Research Article

A novel SEMA3G mutation in two siblings affected by syndromic GnRH deficiency

Roberto Oleari[1§], Valentina André[1§], Antonella Lettieri[1§], Sophia Tahir[2], Lise Roth[3], Alyssa Paganoni[1], Ivano Eberini[1], Chiara Parravicini[1], Valeria Scagliotti[4], Ludovica Cotellessa[5], Francesco Bedogni[6], Lisa Benedetta De Martini[1], Maria Vittoria Corridori[1], Simona Gulli[1], Hellmut G. Augustin[3,6], Carles Gaston-Massuet[4], Khalid Hussain[7*] and Anna Cariboni[1*]

[1] University of Milan, Department of Pharmacological and Biomolecular Sciences, Via Balzaretti 9, 20133 Milan, Italy
[2] Genetics and Genomic Medicine Programme, UCL Great Ormond Street Institute of Child Health University College London, WC1N 1EH, London, UK
[3] Division of Vascular Oncology and Metastasis, German Cancer Research Center (DKFZ-ZMBH Alliance), Im Neuenheimer Feld 280, D-69120 Heidelberg, Germany
[4] Centre for Endocrinology, William Harvey Research Institute, Barts & the London School of Medicine and Dentistry, Barts & the London School of Medicine, Queen Mary University of London, John Vane Science Centre, Charterhouse Square, EC1M 6BQ, London, UK
[5] Department of Clinical Sciences and Community Health, University of Milan, Milan, Italy
IRCCS Istituto Auxologico Italiano, Lab. of Endocrine and Metabolic Research, Milan, Italy
[6] San Raffaele Rett Research Unit, Division of Neuroscience, San Raffaele Scientific Institute, 20132 Milan, Italy
[6] European Center for Angioscience (ECAS), Medical Faculty Mannheim, Heidelberg University, Ludolf-Krehl-Str. 13-17, D-68167 Mannheim, Germany
[7] Sidra Medical & Research Center, Department of Pediatric Medicine, Division of Endocrinology OPC, C6-337 PO Box, 26999 Al Luqta Street, Education City North Campus, Doha, Qatar

[§] These authors contributed equally to the paper

*** Please address correspondence to:**

Professor Anna Cariboni
University of Milan, Department of Pharmacological and Biomolecular Sciences, Via Balzaretti 9, 20133 Milan, Italy
Tel. +39 02 503 18230 E-mail anna.cariboni@unimi.it

Professor Khalid Hussain
Sidra Medical & Research Center, Department of Pediatric Medicine, Division of Endocrinology OPC, C6-337 PO Box, 26999 Al Luqta Street, Education City North Campus, Doha, Qatar
Tel. +974 4003 7608 E-mail khussain@sidra.org

RUNNING TITLE: SEMA3G role in GnRH deficiency

KEYWORDS: hypogonadism, GnRH neurons, SEMA3G

ABSTRACT:

Introduction: Gonadotropin-releasing hormone (GnRH) deficiency causes hypogonadotropic hypogonadism (HH), a rare genetic disorder that impairs sexual reproduction. HH can be due to defective GnRH-secreting neuron development or function and may be associated with other clinical signs in overlapping genetic syndromes. With most of the cases being idiopathic, genetics underlying HH is still largely unknown.

Objective: To assess the contribution of mutated Semaphorin 3G (*SEMA3G*) in the onset of a syndromic form of HH, characterized by intellectual disability and facial dysmorphic features.

Method: By combining homozygosity mapping with exome sequencing, we identified a novel variant in the *SEMA3G* gene. We then applied mouse as a model organism to examine *SEMA3G* expression and its functional requirement *in vivo*. Further, we applied homology modelling *in silico* and cell culture assays *in vitro* to validate the pathogenicity of the identified gene variant.

Results: We found that (i) SEMA3G is expressed along the migratory route of GnRH neurons and in the developing pituitary, (ii) SEMA3G affects GnRH neuron development, but is redundant in the adult hypothalamic-pituitary-gonadal axis, and (iii) mutated SEMA3G alters binding properties *in silico* and *in vitro* to its PlexinA receptors and attenuates its effect on the migration of immortalized GnRH neurons.

Conclusion: *In silico, in vitro* and *in vivo* models revealed that SEMA3G regulates GnRH neuron migration and that its mutation affecting receptor selectivity may be responsible for the HH-related defects.

INTRODUCTION

Puberty onset and sexual reproduction are controlled in mammals by the hypothalamic-pituitary-gonadal (HPG) axis, which is composed of Gonadotropin-releasing hormone (GnRH) neurons in the hypothalamus, gonadotropic cells in the anterior pituitary and sex-steroid producing cells in the gonads (1). The activation and maintenance of the HPG axis depend on the cyclic secretion of the decapeptide GnRH by GnRH neurons, which comprise a small number of cells scattered in a bi-lateral continuum between the olfactory bulbs (OB) and the hypothalamic medial preoptic area (MPOA) (2). GnRH deficiency impairs puberty and leads to infertility, causing a genetic disorder that is known as hypogonadotropic hypogonadism (HH), which is due to defective GnRH neuron development or function (3). For the majority of the patients affected by HH, the underlying genetic loci are unknown (4). Further, GnRH deficiency can be found in combination with other phenotypic features in genetic disorders associated to HH. These include CHARGE (CS), Prader-Willi (PWS) and Bardet-Biedl (BBS) syndromes, which are characterized by a spectrum of additional clinical traits such as eye and ear defects, craniofacial malformations, mental retardation, renal and heart anomalies (5–7).

Here we have identified two brothers affected by an unusual syndrome that includes HH, facial dysmorphic features and developmental delay, born to consanguineous parents and sharing a large region of homozygosity on their genome. By combining homozygosity mapping (HZM) of their DNA with exome sequencing, bioinformatics, functional *in vitro* and *in vivo* studies, we identified a mutation in Semaphorin 3G (*SEMA3G*) and functionally studied its requirement in the GnRH neuron system.

SEMA3G encodes a recently characterized (8) member of the class 3 secreted semaphorin subfamily. To date, other members of SEMA3s and their receptors/co-receptors have already been implicated in the development of the GnRH neuron system (9–11) and in the pathogenesis of HH

(10–16). Yet, the role of SEMA3G in the establishment of the neuroendocrine reproductive axis has not been investigated. Previous mouse work mainly revealed roles for SEMA3G in the patterning of the vascular system (17,18). Accordingly, Sema3g is expressed by endothelial cells and not by neurons or glial cells (19,20). However, endothelial Sema3g can regulate synaptic plasticity of neurons (19). Similar to other class 3 semaphorins, SEMA3G binds to both neuropilins (NRP1-2) (8,18,19) in complexes with plexin A4 (PLXNA4) (19) or D1 (PLXND1) (18).

In this study, we found that *Sema3g* transcript is transiently expressed by endothelial cells associated with migrating GnRH neurons in the nose and that mice lacking *Sema3g* showed a defective migration of GnRH neurons during development. However, adult *Sema3g*-null mice did not phenocopy the reproductive defects observed in our patients. Thus, by studying *in silico* and *in vitro* the effects of SEMA3G mutation, we found that the mutation alters binding affinity and selectivity to its PLXNA co-receptors. In addition, mutated SEMA3G interferes with the binding and the signaling of SEMA3A *ex vivo* and *in vitro*. Further, the mutated SEMA3G is less effective in promoting proliferation, migration and AKT activation in an *in vitro* model of immortalized GnRH neurons.

MATERIALS AND METHODS

Human samples and DNA sequencing. Blood samples were collected from the family through Great Ormond Street Hospital's NHS Trust. Genomic DNA was isolated by standard techniques at the UCL Genomics centre, and the samples were stored at -80°C until analysis.

HZM was conducted by the UCL Genomics services. The Illumina microarray platform was used for the genotyping, following the Infinium HD Ultra Assay protocol (Rev B, 2010, Illumina Inc, San Diego, USA). Results were generated using the Illumina Genomestudio software, and copy number variation and loss of heterozygosity data was generated (cnvPartition v3.1.6, Illumina). The

minimum homozygous region size was 1Mb, with a minimum of 50 consecutive SNPs. Whole exome sequencing was conducted on the 2 patients and their unaffected siblings out of UCL. HZM and exome sequencing data were used simultaneously in patient 2 to identify the candidate gene/mutation lying within the homozygous regions.

Sanger sequencing was performed to detect mutations in the affected patients and their family. Primers were designed using the online Primer3 software. The sequencing reaction was conducted using the BigDye Terminator V1.1 Cycle Sequencing kit (Applied BioSystems, Foster City, CA, USA). The sequences were compared to a reference sequence using the Sequencher® 5.3 software. *In silico* mutational analysis was performed to predict the effect of the mutation.

Mouse strains/approvals. To obtain embryos of defined gestational stages, mice were mated in the evening, and the morning of vaginal plug formation was counted as E0.5. Genotyping of *Sema3g* wild-type or knock-out mice (in C57BL/6 background) was performed by polymerase chain reaction (PCR) (17). Wild-type (CD1 or C57BL/6) or knockout mice were housed in individually ventilated cages under pathogen-free conditions. Animals had free access to food and water and were kept in a 12h light-dark cycle. All procedures were performed in accordance with the European Community Council Directive 86/609/EEC for care and use of experimental animals; all the protocols were approved by local ethical and German home office guidelines, by the UK Animals (Scientific Procedures) Act 1986 as well as by the Italian Minister for Scientific Research and by the local Animal Care Committee.

***In situ* hybridization.** Paraformaldehyde (PFA)-fixed cryosections or paraffin-embedded sections from wild type C57BL/6 animals were incubated with digoxigenin (DIG)-labelled anti-sense riboprobes for mouse *Gnrh* (gift of Dr. Memi)*, Pit1, Pomc1, α-GSU* (21), *Sema3g*. Oligonucleotides used to generate *Sema3g* probe were: Forward: CCTTCATCACAGTGGGGCAT: Reverse: GGTAATACGACTCACTATAGGGATAGGGTCCCCACTGATGCT. The T7 promoter is added at 5' of

reverse primers**.** Specificity of this probe was tested using a sense probe (**Suppl. Fig. 1**). Hybridisation step was performed in hybridization buffer (50% formamide, 0.3M sodium chloride, 20mM Tris HCl, 5mM EDTA, 10% Dextran sulphate, 1x Denhardt's) overnight at 55-65°C depending on probe stringency. Sections were washed with a series of gradually decreasing saline sodium citrate (SSC) buffers and then incubated overnight with AP-conjugated anti-DIG antibody (1:1500; Roche). mRNA expression was revealed by colorimetric staining using 4-Nitro blue tetrazolium chloride solution and 5-Bromo-4-chloro-3-indolyl phosphate disodium salt (NBT/BCIP, Roche).

Histochemical procedures. PFA-fixed cryosections (20 μm thickness) or paraffin-embedded sections (5-10 μm) were incubated for 1h at RT with PBS containing 10% normal goat serum and 0.1% TritonX-100. Cells were fixed for 15min with 4% PFA and then blocked for 30min with 5% normal goat serum and 0.1% TritonX-100. The following primary antibodies, whose specificity was tested in our or other previous works, were used for immunostainings: rabbit anti–peripherin (1:200; AB 1530 EMD Millipore; (9,10)), rabbit anti-GnRH (1:400 for fluorescence and 1:1000 for peroxidase labelling; 20075 Immunostar; (9,10,22)), rabbit anti-S100 (1:500; Z0311 Dako Omnis, Agilent; (23)), mouse anti-Tuj1 (1:500; MMS-435P-250 Covance; (23)), mouse anti-cMyc (1:200; MA1-980 Thermo Fisher Scientific; (10), rabbit anti-PHH3 (1:2000; 9701S Cell Signaling; (24), rabbit anti-caspase 3 (1:200; 9661S Cell Signaling; (25)). Pituitary hormone-producing cells were labelled using the following primary antibodies on 5 μm paraffin-embedded tissue sections: mouse anti-ACTH (1:1000, 10C-CR1096M1 Fitzgerald), rabbit anti-PRL (AFP-425-10-91), -LH (AFP-C697071P), -TSH (AFP-1274789) and -GH (AFP-5641801) (1:500, NHPP, UCLA Medical Centre (26). BV were labelled either with biotinylated-isolectin B4 (IB4) (1:400; Vector Laboratories; (10)) followed by 488- or Cy3-conjugated streptavidin or with rabbit anti-CD31/Pecam (1:50; ab28364 Abcam; (27)) or rat anti-Endomucin (1:300; sc-65495 Santa Cruz; (28)). For testes analysis, testes were embedded in paraffin and sections of 8 μm cut with a microtome. Sections were then stained with haematoxylin and eosin or immunolabelled with an anti-Sox9 antibody (1:1000; gift of Prof. Wegner; (29)) or with a rabbit anti-

Cyp17a1 antibody (1:100; 14447-1-AP Proteintech; (30)). For immunofluorescence staining, secondary antibodies used included 488-conjugated goat anti-mouse IgG (1:400; Jackson Immunoresearch), Cy-3 or 488-conjugated goat anti-rabbit (1:400; Jackson Immunoresearch). Nuclei counterstained with DAPI (1:10000; Sigma-Aldrich). For immunoperoxidase labelling, cryostat or microtome sections were incubated with hydrogen peroxide to quench endogenous peroxidase activity followed by biotinylated goat anti-rabbit, goat anti-mouse or goat anti-rat antibody (1:400; Vector Laboratories) and then developed with the ABC kit (Vector Laboratories) and 3,3-diaminobenzidine (Sigma-Aldrich) as previously described (10). In some experiments, we performed ISH for *Sema3g* before immunostaining for GnRH, Tuj1, S100 or IB4 (31).

Quantitative RT-PCR. RNA was collected from adult P80 testes of wild-type and *Sema3g*-null mice using Trizol-chloroform method. After extraction, 1 µg of RNA for each sample was retrotranscribed and cDNA obtained was used for quantitative (q) PCR analyses as previously described (32). The following primers were used for *Sox9* and *Cyp17a1* respectively (FW 5'-ACGCCTTCATGGTGTGG-3', RV 5'-TCTCGCTCTCGTTCAGCAG-3'; FW 5'-CATCCCACACAAGGCTAACA-3', RV 5' CAGTGCCCAGAGATTGATGA-3'). *Gapdh* was used as housekeeping gene for the normalization of data and the mRNA relative expression was calculated using the mean of wild-type samples as reference.

Homology modeling. Homology modeling of the interaction between human SEMA3G and human PLXNA1-4 was performed with the Molecular Operating Environment (MOE, 2015.10; Chemical Computing Group Inc.). In detail, four complexes of the human SEMA3G and human PLXNAs (SEMA3G::PLXNA1-4) were generated, using as templates the high-resolution mSema3a (PDB CODE 1Q47.A) and mPlxna2 (PDB CODE 3OKY) structures, respectively, to model the single monomers, and the low-resolution mouse Sema3a, Plxna2, Nrp1 complex to guide their reciprocal

orientation/interactions (PDB CODE 4GZA, 7 Å resolution) (33). Amber10:EHT with the reaction field electrostatics treatment was used.

Protein::protein molecular docking. Protein::protein molecular docking was carried out on human SEMA3G with human PLXNAs, producing 4 final complexes (SEMA3G::PLXNA1, SEMA3G::PLXNA2, SEMA3G::PLXNA3, SEMA3G::PLXNA4). The protein::protein docking procedure was validated by reproducing the Sema3a::Plxna2 crystallized complex, used as positive control. The residues of the interaction surfaces were manually selected on the different proteins used in the docking procedure: human SEMA3G (P96-N117; C134-A144; P160-R176; T189-R225; S248-K289; G356-M414), mouse Sema3a (D75; W93-F117; A131-Y143; L157-P173; E185-P224; A251-S257; N271-K288; A357-A401); human PLXNA1 (A46-H53; G66-Y72; A83- G301; G344-P352; L362-E422); human PLXNA2 (S43-H52; G65-Y71; A82-G299; G342-P350; I369-E420); human PLXNA3 (V28-H35; G49-F54; A65-G281; G324-P332; L342-E402) and human PLXNA4 (G45-H53; G66-Y72; T83-G299; G342-L350; L360-R420). The MOE protein-protein docking application was run without any further refinement. Energy was calculated with the GBVI/WSA ΔG empirical scoring function that depends on the average gain/loss of rotational and translational entropy, the selected force field, the coulombic electrostatics using a constant dielectric of ϵ=1, the solvation electrostatics, the van der Waals contribution to binding and the surface area, weighted by exposure. Obtained poses were analyzed by superposing to model and scored by energy.

Mutant generation and analysis. The p.G166V mutation was introduced in all the generated complex models through the MOE Protein Design tool. The conformational space of the mutant *vs* the wild-type complexes was efficiently explored through low mode molecular dynamics (MD) simulations that allow sampling of an ensemble of rotational conformers both of mutated and of the surrounding amino acids, using the implicit solvation for minimizing and rearranging the lateral chains of wild-type and mutated SEMA3G. According to the default procedure, all atoms of the

mutated residue were left free to move; to avoid larger changes in the backbone conformation, backbone of residues within 4.5 Å were tethered. Residues farther than 4.5 Å were fixed and, to speed up the simulation, atoms farther than the non-bonded cutoff > 5 Å were marked as inert. After an ensemble is generated, conformations within an RMSD value < 0.25 Å (i.e., similar conformations) were removed. The remaining conformations were then scored and sorted using the stability scoring function. Conformations with relative energies of the global minimum higher than 10 kcal/mol were removed. Additionally, only the best 25 conformations were kept. All properties and scores are then averaged using the Boltzmann's distribution. Amber10:EHT force field, with the Generalized Born implicit solvent model was used.

Solvation studies. Solvation energy is calculated with the MOE potential energy tool. E_{sol} is the implicit solvation energy calculated using the Generalized Born model (GB/VI).

Solvent distribution analysis was performed using the MOE 3D-Reference Interaction Site Model (3D-RISM) tool.

Cell lines. GN11 cells (gift from Prof. Radovick (34)) and COS-7 cells (ATCC) were grown in standard conditions (Dulbecco's MEM containing 1 mM sodium pyruvate, 100 mg/ml streptomycin, 100 U/ml penicillin and 10% FBS; Invitrogen). Cells were checked for mycoplasma contamination (MycoAlert Detection Kit, Lonza) monthly and were contamination-free.

Expression vectors and conditioned media. The expression vectors for hPLXNA1 and A4 were kindly provided by Dr. Andrews. To introduce the c.497G>T (p.G166V) mutation into human *SEMA3G* gene, we mutated the expression vector using the QuickChange Lightning Site-Directed Mutagenesis Kit (Agilent Technologies) and the oligonucleotides FW 5'-ACCGCCCCCGGACACTTTCCACACTGC-3' and RV 5'-GCAGTGTGGAAAGTGTCCGGGGGCGGT-3'. Expression vectors were transiently transfected into COS-7 cells using Lipofectamine 2000 (Invitrogen). Transfection efficiency was determined from 3 independent transfections as a ratio of fluorescent positive cells to the total of DAPI positive cells

number. Conditioned media were collected 48 h after transfection and, if needed, concentrated by diafiltration with Microcon-30kDa Centrifugal Filter Unit (Millipore).

Immunoblotting. Cells were lysed in 150 mM NaCl, 50 mM Tris-HCl (pH 7.4) and 1% Triton X-100, supplemented with protease and phosphatase inhibitors (Roche). Lysates were centrifuged at 13,000 rpm for 10min at 4°C and protein concentration determined with the Bradford assay (BIO-RAD). Concentrated CM of transfected COS-7 cells were diluted 1:2 in Laemmli sample buffer (35). 20 µg of protein lysate or 20 µL of concentrated conditioned media were used for SDS-PAGE; prestained Sharpmass VII (Euroclone) was used as protein molecular weight marker. Proteins were transferred to nitrocellulose membrane (BIO-RAD) and immunoblotted with the following antibodies: anti-cMyc (1:1000; Thermo Fisher Scientific (10)), rabbit anti-pAKT Ser473, rabbit anti-AKT (1:1000 each; 9271 and 9272 Cell Signalling (10)) followed by secondary horseradish peroxidase-conjugated anti-rabbit or anti-mouse antibodies (1:10000; Santa Cruz Biotechnology). Densitometric analysis of band intensity was performed using the Image J and the mean pixel intensity calculated. AKT/pAKT ratio was calculated and results represented as percentage in activation compared to the maximum value fixed as 100% of 3 independent experiments.

Alkaline phosphatase (AP)-fusion protein-binding assay. COS-7, GN11 cells or WT E14.5 mouse sections were fixed for 5min in methanol, washed 5 times with PBS, incubated in PBS containing 10% FBS for 30min, and then reacted with AP fusion proteins (SEMA3A, SEMA3G WT or mutant) for 2h at room temperature, as previously described (9). For competitive assays, sections were first pre-incubated with mutant SEMA3G-CM overnight and then reacted with SEMA3A-CM. Cells or sections were then washed for 5min each with PBS, fixed with 4% PFA for 2min at room temperature, and washed again. Endogenous AP was heat-inactivated by incubation at 65°C for 2h. Cell-bound, heat-stable protein-AP activity was detected as an insoluble reaction product after incubation with 4-

nitro blue tetrazolium chloride (NBT) and 5-bromo-4-chloro-3-indolyl phosphate (BCIP) (Roche). Images were recorded using Zeiss Axioskop2 plus microscope equipped with a digital camera.

Migration assays. Subconfluent GN11 cells were used for chemotaxis experiments using a 48-well Boyden's chamber (Neuro Probe). For these experiments, GN11 cells were suspended in serum-free medium (10^5 cells/50 µL) and placed in the upper compartment of the Boyden chamber. Compartments were separated by a polycarbonate porous membrane (8 µm pores) pre-coated with gelatin (0.2 mg/mL). 28 µL of with the concentrated CM from COS-7 cells transfected with control expression vector or with expression vectors for SEMA3G, SEMA3G^{G166V} or SEMA3A were placed into the lower compartment of the chamber. The chamber was kept in an incubator at 37°C for 2h. After 2h, cells that had migrated through the membrane separating the two compartments of the chamber were stained using the Diff-Quick kit (Biomap, Italy). Images were taken using a Zeiss Axioskop2 plus microscope with a 20× objective and analyzed with ISCapture software. Three random fields of stained cells were counted for each well, and the chemomigration expressed as relative fold-increase compared to the control-CM whose value was fixed to 1, from ≥3 independent experiments.

Proliferation assays. GN11 cells were seeded in 24-well plates at a density of 5000 cells/well and grown for 24h in standard conditions (Dulbecco's MEM containing 1 mM sodium pyruvate, 100 mg/ml streptomycin, 100 U/ml penicillin and 10% FBS; Invitrogen). For proliferation assays, cells were cultured overnight without serum and then for 24h in the presence of control CM or CM expressing wild-type or mutated SEMA3G. We then determined the percentage of phospho-histone H3 (PHH3)-positive cells out of all DAPI-positive cells for each treatment group in 12 random pictures from 3 independent experiments.

Image processing and quantifications. We used a Zeiss Axioskop2 plus microscope equipped with a TCH-5.0ICE digital camera to acquire bright-field images and a Leica TCS SPE1 confocal microscope

to acquire fluorescent images. All images were processed using Photoshop CS4 (Adobe Inc.). In some experiments, we combined bright-field images of ISH stainings with images of immunofluorescence staining after they were acquired on the same microscope; after imaging, the bright-field images were inverted and converted to RGB colour mode for superimposition with the confocal images. To determine the total number of GnRH neurons in E14.5 mouse heads or P80 mouse MPOA, 20 µm sagittal sections through each entire head/MPOA were immunolabelled for GnRH and all GnRH-positive cells counted in each section, as previously described (9). For each genotype, we analysed at least three embryos, and all GnRH-positive cells were counted in each section of each head under a 40× objective. To quantify GnRH innervation of the ME, we calculated the percentage of stained area for each 20 µm-section over the whole ME of 3 mice for each genotype with ImageJ software. Bound AP-conjugated proteins to COS-7 cells overexpressing PLXNA1-4 was measured using the ImageJ software; control-CM has been used as baseline to calculate the fold change for each condition.

Statistics. For all experiments, we calculated the mean of at least three independent samples. Data are expressed as mean ± standard error of the mean (s.e.m.). To determine statistical significance, we used the two-sided unpaired Student's *t* test or, for multiple comparison, a One-way ANOVA followed by a Tukey post-hoc test or Two-way ANOVA followed by Bonferroni post-hoc test. A p-value of < 0.05 (one asterisk) was considered significant; a p-value of < 0.01 was indicated with 2 asterisks, a p-value of < 0.001 with 3 asterisks. Statistical analysis was performed using Prism4 (GraphPad Software).

RESULTS

Two siblings from consanguineous parents show reproductive defects, dysmorphic features and developmental delay.

We identified a patient with an unusual syndrome characterized by cryptorchidism, a poorly

developed scrotum, HH and facial dysmorphic features. The patient belonged to a consanguineous family of Pakistani origin, in which the parents were first cousins. He had a younger brother with similar features, and two elder sisters unaffected by the condition. The family pedigree is outlined in **Fig. 1A**.

The proband (patient 1) was a 20-year-old male, who was born at 41 weeks of gestation after a normal delivery, with a birth weight of 2.8 kg. At birth, he presented with bilateral undescended testes, normal phallus, and a poorly developed scrotum. Bilateral orchidopexy was performed at 4 years of age. He was subsequently noted to have very small bilateral atrophic underdeveloped testes and a small hypoplastic scrotum. Dysmorphic facial features noted in the patient include unusual prominent staring eyes, prominent nasal bridge, brachycephaly, synorphrys, a beaked nose. small mouth and chin, a high palate and pointed ears with an over folded helix.

A human chorionic gonadotropin (hCG) test performed at the age of 3.7 years showed a normal testosterone response with a peak at 14.5 nmol/L from a basal level of less than 0.7 nmol/L, confirming that the gonads are functioning well and are producing testosterone when stimulated. A GnRH test performed at the age of 3.7 years showed follicle-stimulating hormone (FSH) and luteinizing hormone (LH) levels of 4.1 IU/L for both hormones, as maximum response after stimulation. A 3-week hCG test performed at 11 years of age also showed a normal response with a maximum testosterone response of 19.5 nmol/L. Further, growth hormone (GH) stimulation test showed a maximum growth hormone response of 14.0 ng/mL. A diagnosis of HH, which is typically made at adolescence and characterized by low levels of testosterone in male individuals in the setting of low or normal levels of gonadotropins (LH and FSH) (4), was made at 15 years of age. Specifically, the proband presented with testicular volumes of 3 mL (right testis) and 2 mL (left testis) (testicular volume <4 mL at the age of 14 years indicates absent puberty; (4)), testosterone levels of 0.9 nmol/L (normal levels at 14-15 years 3.5-18.7 nmol/L, (36)) and gonadotropin levels of 0.5 IU/L (FSH) and 0.6 (LH) (normal levels: FSH 1.9-12.4 and LH 2.0-8.6, (37)). At the same age a patient's

height velocity of 4.0 cm per year was determined. During a follow-up visit after 7-months of testosterone and gonadotropin treatment, the patient's testicular volumes increased to 5 mL and 4 mL, respectively, and height velocity to 5.4 cm per year.

Further testosterone injections (50 mg every four weeks) resulted in the linear growth and development of secondary sexual characteristics, leading to pubic and axillary hair growth and an increase in penile size in the patient. The proband attained the expected mid-parental height.

The younger brother was a 15-year-old male who was born at 36 weeks of gestation with an emergency lower segment caesarean section. The birth weight was not recorded. Antenatal scans showed a dilated large bowel, oligohydramnios and microcephaly. At birth, he presented with an anorectal malformation, and colostomy was performed at day 2 after birth. Subsequently, posterior sagittal anorectoplasty was performed at 1 year of age, followed by colostomy closure in the same year. The patient had bilateral undescended testes and a small phallus. Right orchidopexy was performed initially. Since the left testis was not palpable, left orchidopexy was performed later at the age of 9 years. The patient had also a hypoplastic scrotum. A hCG test performed at the age of 2.7 years showed a normal testosterone response with a peak at 28.3 nmol/L from a basal level of less than 0.7 nmol/L. A GnRH test performed at the same age showed FSH and LH levels of 2.4 IU/L and 1.4 IU/L, respectively, as maximum response upon stimulation. A 3-week hCG test showed a maximum testosterone response of 22.2 nmol/L.

The dysmorphic features of this patient included a small round head, beaked nose, and thin upper lips. The left helix was slightly unfolded, and the ear was slightly protruding. Growth hormone (GH) stimulation test (glucagon) in the patient with a maximum growth hormone response of 4.2 ng/mL, which combined with low IGF-1 serum levels (50 ug/dL; references range 150-400 ug/dL, (38)) suggested GH deficiency. Growth velocity 6 months after starting GH treatment, at 6 years old, was 10 cm/year (normal 4-6 cm/year). Notably, sibling 2 attained height -1.0 SD below the mid-parental height.

Both patients were noted to have some developmental delay. Patient 1, at 5 years of age had a general development quotient of 60 in the severely delayed range. He had significant learning difficulties, was unable to speak in sentences and at 8 years of age was enrolled in a specialized school. Patient 2 began to walk at 2 years and 7 months and was not speaking by the age of 3 years. MRI of their brains as well as hearing and olfaction were normal in both brothers. The prolactin levels were normal and there were no features of hemochromatosis in both patients. The combination of the clinical features described above suggests that the two brothers may have a novel syndrome, as the constellation of these features has not been previously described.

A point mutation in the SEMA3G gene was found in the two affected brothers.

Due to the unique presenting features of the two patients including the birth from consanguineous parents, an autosomal recessive disease with a homozygous genetic pattern of inheritance was suspected. HZM was performed on the two patients and their two unaffected sisters to identify candidate genes, followed by exome sequencing. The shared homozygous regions found in the affected patients, and absent in the unaffected siblings, are presented in **Table 1**. In total, the affected brothers shared approximately 85 Mb of unique homozygous region which contained over 600 protein-coding genes. The largest shared region, around 38 Mb, was found on chromosome 3 (**Table 1** and **Fig. 1B**).

Variants from exome sequencing data found in the homozygous regions were filtered to narrow down the list of variants. First, the variants that disrupted gene function, by causing a non-synonymous or a stop gain change in the protein coding sequence, or affected the splice site, were identified. The remaining variants were filtered out. The homozygosity mapping data were next used in conjunction with the filtered variants to identify those lying within all the shared homozygous regions. As we hypothesized an autosomal recessive disorder, we next filtered for homozygous mutations in these regions. Finally, the variants found in a homozygous state in SNPs

databases (dbSNP130 and 1000 Genomes project) were filtered out, leaving those unique to the patients, within the shared homozygous regions. Specifically, this analysis identified *SEMA3G* as a potential candidate gene, with nucleotide change c.497G>T and protein change p.Gly166Val (p.G166V). This variant had previously been reported in databases such as gnomAD, ExAC and dbSNP (rs549122188) with global minor allele frequencies (MAF) < 0.05%; yet, no homozygous variants have been reported so far.

As class 3 semaphorins and their receptors have been extensively implicated in the pathogenesis of HH and in the GnRH neuron physiology (14,15), we considered *SEMA3G* as the main candidate to explain the HH phenotype in our patient. In addition, no mutations in known HH genes were found. Sanger sequencing confirmed the novel change to be present in the homozygous state in the two affected patients. Both parents and the eldest sister were heterozygous carriers for the mutation, and the second sister was homozygous for the normal reference allele (**Fig. 1C**). The c.497G>T (p.G166V) mutation substitutes an ambivalent glycine residue with a hydrophobic valine residue and is predicted to be possibly damaging and disease causing according to PolyPhen (39), SIFT (40) and MutationTaster (41) bioinformatic tools, respectively (**Fig. 1D**). The p.G166V mutation resides in the SEMA domain which is characterized by a conserved set of cysteine residues, forming four disulphide bonds that stabilize the structure (**Fig. 1E**). The mutated residue affects a glycine residue that is conserved between vertebrates (**Fig. 1F**).

Sema3g expression during mouse GnRH neuron and pituitary development.

Because other class 3 semaphorins and their receptors/co-receptors NRPs/PLXNs are implicated in mouse GnRH neuron development and in the pathogenesis of HH (11,15), we applied mouse as model organism to study the expression pattern of *Sema3g* and its functional requirement in the GnRH neuron system. In wild-type mice, GnRH neurons are first detected at embryonic day

(E) 10.5 in the nasal pit, migrate in the nasal compartment and then in the basal forebrain, where they reach the hypothalamus. The migration starts at approximately E11.5 and it is completed just before birth (42). Thus, to get insights into the expression pattern of *Sema3g* during GnRH neuron development, we performed *in situ* hybridization (ISH) for *Gnrh* and *Sema3g* on adjacent sections, at E12.5, E13.5 and E14.5. As shown in **Suppl. Fig. 2**, *Sema3g* was expressed between E12.5 and E14.5 along the nasal septum in areas including the migratory path of GnRH neurons (43). This expression pattern suggested a possible role of Sema3g in the navigation of GnRH neurons in the nasal compartment. To check whether the *Sema3g*$^{+}$ cells were GnRH neurons, we performed double *in situ*-immunofluorescence protocols using the *Sema3g* probe and an anti-GnRH antibody. We found that these two cell populations were distinct with no co-expression of *Sema3g* in GnRH neurons (**Fig. 2A**). Thus, to further characterize the cell type expressing *Sema3g* along the GnRH neuron migration in the nose, we performed similar experiments with markers for neurons (Tuj1) **(Fig. 2B**), olfactory ensheathing cells (OECs; S100) (**Fig. 2C**) or blood vessels (isolectin-B4, IB4) (**Fig. 2D**). In agreement with previous reports (19,20) we found that *Sema3g*-expressing cells were endothelial cells, as evidenced by the co-localization of *Sema3g* mRNA and the IB4 staining (**Fig. 2D**). We also found expression of *Sema3g* mRNA transcripts in the developing hypothalamus and pituitary (**Fig. 2E-I**). Notably, expression of *Sema3g* was detected in the anterior lobe of the developing pituitary gland with a peak of expression at E12.5 (**Fig. 2F**). *Sema3g* was also expressed in the ventral and anterior hypothalamic region at this stage, and expression declined at E18.5 (**Fig. 2I**).

These observations were consistent with a possible requirement for Sema3g during GnRH neuron migration from the nasal compartment to the hypothalamus as well as in the developing pituitary. We therefore examined GnRH neuron migration and pituitary development in *Sema3g*-null mice.

Sema3g loss affects the development of GnRH neurons and pituitary

As patients carry homozygous mutation of *SEMA3G* (**Fig. 1**) and we detected expression of *Sema3g* in the nasal compartment (**Fig. 2**), we first asked if *Sema3g*-null mice (17) showed impaired GnRH neuron development. Immunohistochemical GnRH staining of coronal sections followed by counting the GnRH-positive cells in each head demonstrated a reduced number of GnRH neurons in mutants compared to wild-type mice at E14.5 (**Fig. 3**; GnRH neuron number ± s.e.m.; *Sema3g*$^{+/+}$ 1172.0±80.3 vs. *Sema3g*$^{-/-}$ 811.3±44.8; ***** p=0.017; two-sided unpaired Student's *t* test, n=3 for each group). Because GnRH neurons at E14.5 can be observed in the nose, in the nasal-forebrain junction (NFJ) and in the forebrain (FB), we next determined the relative number of neurons in these three compartments. We observed a similar number of GnRH-positive cells in the nose and in the NFJ of mutants compared to wild-types, with a significantly reduced number in the FB of mutants compared to wild-type mice (**Fig. 3A-B;** nose: *Sema3g*$^{+/+}$ 366.0±68.0 vs. *Semag3*$^{-/-}$ 342.0±42.7, p>0.05; nfj: *Sema3g*$^{+/+}$ 295.3±27.2 vs *Semag3*$^{-/-}$ 244.7±15.6, p>0.05; fb: *Sema3g*$^{+/+}$ 511.0±31.3 vs. *Sema3g*$^{-/-}$ 224.7±34.1, ****** p=0.004; two-sided unpaired Student's *t* test, n=3 for each group). We therefore examined whether Sema3g was required for the survival of GnRH neurons in the developing brain. For this analysis, we labelled adjacent coronal sections through the MPOA, where most GnRH neurons reside at E14.5, with antibodies against GnRH or activated caspase-3, a marker for cells committed to undergo apoptosis. As shown in **Suppl. Fig. 3A**, we did not detect apoptotic cells in the forebrain of either wild-type or *Sema3g*$^{-/-}$ mice, thus excluding that the reduced number of GnRH neurons in the forebrain may be due to GnRH neuron cell death via apoptosis. Activation of caspase-3 was detected at normal levels in the salivary gland, used as positive control (44), of both genotypes **(Suppl. Fig. 3A).**

To assess whether the GnRH neuron migration defect observed in knockout mice could be

due to alterations in the patterning of blood vessels (BV) and olfactory/vomeronasal (OLF/VN) axons present in the nasal compartment (9,24), we stained the BV and OLF/VN nerves of wild type and *Sema3g*$^{-/-}$ mice for IB4 and peripherin, respectively. We observed the presence of BV without overt vascular defects (**Suppl. Fig. 3B**) and normal patterning of OLF/VN axons (**Suppl. Fig. 3C**), in *Sema3g*-null mice compared to wild-types. Similarly, immunostainings for Endomucin and Pecam did not reveal differences in the patterning of BV in the developing pituitary of mutant compared to wild-type littermates at E14.5 (**Suppl. Fig. 4**).

Taken together, these data are consistent with a primary direct role for Sema3g signaling in GnRH neurons, rather than indirect effects of Sema3g-dependent OLF/VN nerves or BV on GnRH neuron development.

In addition, because *Sema3g* was also expressed in the developing pituitary (**Fig. 2B**), we analyzed the expression of pituitary cell lineage commitment markers in *Sema3g*$^{-/-}$ embryos to assess if Sema3g might also control pituitary development. Specifically, by using ISH, we analyzed the expression of *Pit1,* which is required for somatotrophs, thyrotrophs and lactotrophs (45–47), *Pomc1,* which gives rise to corticotrophs and melanotrophs (48,49) and the α-glycoprotein subunit (*α-GSU*), which is expressed by gonadotrophs and Pit1-independent thyrotophs (50). No differences were observed in the expression of *Pomc1* (**Fig. 3C**)*,* whereas we observed a modest reduction of *α-GSU* and *Pit1* at E14.5 in the *Sema3g*$^{-/-}$ pituitaries compared to wild-type littermates. These observations are consistent with a developmental delay in the differentiation of some pituitary cell lineages, however terminal differentiation of hormone producing cells was not affected.

Hypothalamic GnRH neuron number, pituitary gonadotrope cells and testes morphology are normal in the adult Sema3g-null mice

To evaluate whether the developmental defects of GnRH neurons observed in *Sema3g*-null mice during fetal life impact adult fertility, we analyzed the HPG axis of *Sema3g*-null mice. In adults,

GnRH neurons are mainly located in the MPOA of the hypothalamus and project to the median eminence (ME), where they release GnRH into the portal BV of the pituitary. We therefore analyzed the GnRH neuron complement in the hypothalamus of adult (P80) *Sema3g*-null mice and observed a small but not significant reduction in the number of GnRH neurons reaching the MPOA in mutants compared to wild-types (**Fig. 4A,B;** GnRH neurons ± s.e.m.; MPOA: *Sema3g*$^{+/+}$ 353.8±39.7 vs. *Semag3*$^{-/-}$ 298.0±31.8, p>0.05, p=0.315; two-sided unpaired Student's *t* test, n=4 for each group). Yet, the innervation of the ME appeared normal in both genotypes, as confirmed by measuring pixel intensity of the GnRH immunoreactive neurites (**Fig. 4A,B;** % of stained area: *Sema3g*$^{+/+}$ 1.9±0.2 vs. *Semag3*$^{-/-}$ 2.1±0.3; p>0.05, p=0.195; two-sided unpaired Student's *t* test, n=4 for each group).

Consistent with a normal innervation of the ME, we did not observe any differences in the expression of terminally differentiated hormone-producing cells in the adult (P80) pituitary gland of the *Sema3g*$^{-/-}$ mutant animals compared to wild-type control littermates (**Fig. 4C**). Similarly, the size and morphology of wild-type and mutant testes were overall normal (**Fig. 4D**). Although histological examination of sections stained with H&E revealed a small but significant reduction in the density of seminiferous tubules (mean count/mm^2 ± s.e.m.; *Sema3g*$^{+/+}$ 16.3±0.8; *Semag3*$^{-/-}$ 14.2±0.5; ***** p=0.032; Student's *t* -test, n=3 for each group), Sertoli cells (stained with an anti-Sox9 antibody) and Leydig cells (stained with an anti-Cyp17a1 antibody) appeared normal in both genotypes. Consistently, qPCR experiments (**Fig. 4E**) showed normal levels of *Sox9* and *Cyp17a1* in both genotypes (*Cyp17a1* relative expression: *Sema3g*$^{+/+}$ 0.9±0.1 vs *Sema3g*$^{-/-}$ 0.8±0.23, p=0.580; *Sox9* relative expression: *Sema3g*$^{+/+}$ 1.0±0.03 vs *Sema3g*$^{-/-}$ 0.9 ± 0.2, p=0.482; n=3 for each group, two-sided unpaired Student's *t* test).

Overall, although we found that Sema3g was expressed during fetal life and its loss affected GnRH neuron development, a normal HPG axis was reached in adult *Sema3g* null mice.

The p.G166V mutation affects the affinity of SEMA3G to its PLXNA receptors in silico.

Because the analysis of homozygous null mice did not fully phenocopy the GnRH deficiency present in the brothers carrying SEMA3G^{G166V} mutation, we first studied the possible effect of the mutation *in silico*, by computational modelling. According to the available modelling data, class 3 semaphorins bind as a dimer to a receptor complex formed by two plexins and two neuropilins (33). Thus, to predict the possible impact of the *SEMA3G* mutation on binding properties and stability of this ternary complex, we first performed *in silico* modelling studies.

To date, mouse Semaphorin 3A (mSema3a) is the only class 3 semaphorin co-crystallized in a ternary complex with mouse Neuropilin-1 (mNrp1) and Plexin A2 (mPlxna2) and shares 46% identity with hSEMA3G, making it a suitable template for homology modelling (51,52). Thus, to investigate the affinity of wild-type SEMA3G for the different PLXNAs, four comparative models of the SEMA3G::PLXNA1-4 complexes were built and their relative orientation was checked through protein::protein docking. Binding free energy results indicated that SEMA3G binds in order of affinity to PLXNA4 (ΔG = -19.2 kcal/mol), PLXNA3 (ΔG = -17.6 kcal/mol), PLXNA1 (ΔG = -15.6 kcal/mol) and PLXNA2 (ΔG = -10.9 kcal/mol).

Modelling data also predicted that the SEMA3G^{G166V} mutation located at the interaction interface between SEMA3G and PLXNAs. Thus, the impact of the mutated residue on protein stability was evaluated through Low Mode Molecular Dynamics (MD), which allows to predict changes in protein stability upon mutation based on a scoring function trained on over 3000 single point reported mutations (53,54). Interestingly, we found that the mutation overall stabilizes the formation of all the four complexes and induces an increase in affinity for all four PLXNAs (**Table 2**), with the greatest value for PLXNA1 (Δ Affinity = -8.2 kcal/mol). To further characterize the impact of mutation on the binding to PLXNA1, which is implicated in HH, subsequent analyses were therefore focused on the SEMA3G::PLXNA1 complex (**Suppl. Fig. 5**).

To better describe the contribution of each residue at the interaction interface between SEMA3G and PLXNA1, a protein contact analysis was carried out on Boltzmann's average structures generated by the conformational sampling of the residues around the mutation and provided by the Low Mode MD approach. Compared to SEMA3G^{G166V}, wild-type SEMA3G showed a different network of interactions with PLXNA1 (**Suppl. Table 1**), likely due to a backbone rearrangement upon mutation rather than to a direct interaction of Gly or Val 166 with PLXNA1. For example, in wild-type SEMA3G, Arg167 can form two ionic interactions and a hydrogen bond with PLXNA1 Asp410, whereas Arg167 of mutated SEMA3G can only form one ionic interaction with PLXNA1 Asp410 (**Fig. 5A**, upper panels). Besides Arg167, other residues contribute to the interaction between SEMA3G and PLXNA1; however most of these residues are distributed along the whole interaction interface and far from the mutated residue (**Suppl. Table 1**). Overall, the analysis of contributions of each single interaction to the affinity of SEMA3G for PLXNA1 resulted in an energetic gain of -1.9 kcal/mol for SEMA3G mutant vs. the wild-type form. Although the Low Mode MD method predicted an affinity gain value that is approximately 4-fold higher compared to this value (-8.2 kcal/mol vs -1.9 kcal/mol), the different results could be due to the effect of solvation in the affinity calculations through the use of the Generalized Born (GB) implicit solvent model (55). In line with this hypothesis, the solvation analysis showed that the overall solvation energy is more favorable in the wild-type complex, with a difference of approx. -87.0 kcal/mol. Conversely, the mutant complex showed a gain in solvation energy of -39.6 kcal/mol, of which only -9.9 kcal/mol are ascribable to V166. These results suggest that the p.G166V mutation increases SEMA3G affinity by reducing solvation energy of the interacting amino acids without influencing the amino acid interaction network. Consistent with this result, the solvation of unbounded SEMA3G wild-type seems to be favored (wild-type = -1789.8 kcal/mol *vs* SEMA3G^{G166V} = -1569.0 kcal/mol).

Further, by applying a 3D-Reference Interaction Site Model (RISM), which provides the solvent structure in the form of a 3D site distribution function, the presence of a cluster of water molecules

(blue mesh surface) around the position of the mutation was found in both WT and mutated SEMA3G. The two complexes also presented a different extension of positive free energy at the surface (solid red), suggesting that the increased affinity of SEMA3G^{G166V} for PLXNA1 could also depend on water reorganization around the mutated residue. The analysis of the water-accessible surfaces showed then a positively-charged patch around the mutation area, that was significantly higher for SEMA3G^{G166V} compared to wild-type (**Table 3**, mutant 284.3 Å^2, wild-type 167.6 Å^2, shown in blue in **Fig. 5A**, lower panels).

In summary, our *in silico* analyses showed that the mutation was likely to induce a change in receptor binding selectivity with a significant increase in the binding affinity of mutated SEMA3G for its canonical ligand PLXNA4 and ectopically to PLXNA1. This could be due to the ability of the p.G166V mutation to induce a local rearrangement of the surrounding amino acids and water molecules, and to the stabilizing effect of the positive patches.

SEMA3G^{G166V} binds to PLXNA1-expressing COS-7 cells with higher affinity compared to wild type.

To corroborate the *in silico* findings and to test whether the mutation found in the patients determined an increased affinity for PLXNA1 also *in vitro*, we set up binding assays on PLXNA4 or PLXNA1-overexpressing cells using alkaline-phosphatase (AP)-conjugated c-Myc-tagged human SEMA3G (17) and SEMA3G^{G166V} ligands.

We first performed immunostainings and immunoblotting assays using an anti-c-Myc antibody to establish that both proteins were expressed and effectively secreted in COS-7 cells (**Fig. 5B,C**). We then used the conditioned medium (CM) of COS-7 cells expressing wild-type (17) or mutated SEMA3G for binding assays on COS-7 transiently expressing human PLXNA4 or PLXNA1. Both wild-type SEMA3G and SEMA3G^{G166V} bound to PLXNA4 or PLXNA1-expressing COS-7 cells (fold change of integrated density vs control-CM: wild-type SEMA3G 89.3±36.8, SEMA3G^{G166V} 296.5±71.1 for

PLXNA4; wild-type SEMA3G 20.9±5.1, SEMA3G^{G166V} 117.6±20.2 for PLXNA1; Fig. 5D). Moreover, and in agreement with the *in silico* predictions, the mutated one bound 3-fold and 6-fold more to PLXNA4 and PLXNA1, respectively, compared to the wild-type (Fig. 5D), as shown by a more intense staining of the reacted cells (fold change of SEMA3G^{G166V} vs wild-type SEMA3G: 3.3±0.8 PLXNA4, *p=0.038; PLXNA1 5.6±1.0, **p=0.004; n=4 for wild-type SEMA3G; n=3 for SEMA3G^{G166V}; two-sided unpaired Student's *t* test).

Taken together, these results confirmed that the p.G166V mutation altered receptor binding properties and affinities by making the SEMA3G protein highly affine for its canonical receptor PLXNA4 but also for PLXNA1. These results are also suggestive of a potential action *in vivo* of mutated SEMA3G, which could interfere with other PLXNA1-mediated signaling molecules such as SEMA3A, known to be essential for GnRH neuron migration (9,11,16).

SEMA3G^{G166V} interferes with SEMA3A binding to embryonic nasal and forebrain tissues

To test this hypothesis, we performed competitive binding assays also *in vivo* with SEMA3A-AP on normal tissues or tissues pre-incubated with mutant SEMA3G. We confirmed that SEMA3A binds on the nasal tissue of E14.5 mouse sections (9) as well as on the striatum and on the cortex of E14.5 sections (**Fig. 5E**, left panels) (56). Instead, when the sections were pre-absorbed with SEMA3G^{G166V}, the enzymatic reaction of the AP-bound SEMA3A was less efficient (**Fig. 5E,** right panels). Although qualitative, these results suggest that mutated SEMA3G may interfere with other SEMA3-signals that are essential for GnRH neuron development to indirectly cause GnRH deficiency.

Mutated SEMA3G protein affects GN11 cell behavior and response to SEMA3A.

Because we observed that *Sema3g* was physiologically expressed in the nasal compartment where

it affected GnRH neuron development, we used GN11 as an established model of immature migrating GnRH neurons (34) to study the cellular and biochemical mechanisms through which wild-type and mutated SEMA3G may affect GnRH neurons.

Because GN11 express *Nrp1* and *Nrp2* (57) as well as *Plxna1*, *Plxna2*, *Plxna3* and *Plxna4* (**Fig. 6A**) receptors, these cells represent a suitable model to study the effects of wild-type vs mutated SEMA3G. We first tested binding abilities of wild-type and mutated SEMA3G-CM and we did not find differences (**Fig. 6B**), possibly because GN11 cells express all the SEMA3G receptors and co-receptors making difficult to detect altered binding properties to the different single receptors. We then used GN11 cells to study the effects of SEMA3G on the migratory activity of GnRH neurons because GN11 show a strong chemomigratory response *in vitro* (24,55). For these experiments, GN11 neurons were exposed to control CM or to CM of COS-7 cells transfected with wild-type or mutated SEMA3G for 2h. We found that the chemomigration of GN11 cells was significantly increased in the presence of wild-type SEMA3G compared to control (CTRL) media. Instead the difference between CTRL and mutant SEMA3G did not achieve statistical significance (expressed as relative migration vs control-CM: wild-type SEMA3G 1.**5**±0.1; SEMA3G^{G166V} 1.2±0.1; CTRL vs WT ** p=0.**003**; CTRL vs G166V p=0.25**1**; WT vs G166V P=0.08**5** ; One-way ANOVA followed by Tuckey post-hoc test, n=7) (**Fig. 6C**).

Further, to investigate whether the mutated protein might interfere with SEMA3A also in this cellular model, GN11 cells were exposed to SEMA3A alone or in the presence of WT or mutant SEMA3G. As expected, SEMA3A inhibits the chemomigration of GN11 cells (9); a similar effect is still observed in the co-presence of SEMA3A and WT SEMA3G suggesting that the WT SEMA3G does not compete with SEMA3A. Instead, when GN11 cells were co-exposed to SEMA3A and mutant SEMA3G the inhibitory effect of SEMA3A was almost abolished, with a number of migrated cells that was similar to the control media (expressed as relative migration vs control-CM: SEMA3A 0.5±0.04; SEMA3A+WT SEMA3G 0.5±0.1; SEMA3A+SEMA3G^{G166V} 0.9±0.2; CTRL vs 3A * p=0.011; CTRL vs

3A+3G WT * p=0.011; CTRL vs 3A+3G G166V p=0.808 ; 3A vs 3A+3G G166V * p=0.035; 3A+3G WT vs 3A+3G G166V * p=0.038; One-way ANOVA followed by Tukey post-hoc test, n=3).

Altogether these results suggested that mutant SEMA3G was less effective in promoting GN11 cell migration and prevented the effects of SEMA3A, likely by its binding to PLXNA1 receptor.

To study the effects of p.G166V mutation on the activation of signaling pathways previously implicated as downstream effectors of semaphorins in GnRH neuron cell lines, we analyzed the activation of AKT (10,12,58) in GN11 treated with wild-type or mutated SEMA3G. GN11 cells were serum-starved overnight and then treated with concentrated CM (wild-type SEMA3G and SEMA3G^{G166V}) for 5-60min. We observed that wild-type SEMA3G could induce the activation of AKT with a peak after 60min, whereas SEMA3G^{G166V} was less effective (mean of the relative percentages of activation ± s.e.m: WT 5': 49.3±2.9; WT 15': 55.3±3.6; WT 30': 78.3±6.4; WT 60': 100; MUT 5': 18.**4**±1.7; MUT 15': **21.0**±7.8; MUT 30': 36.9±14.4; MUT 60': 53.3±9.6; WT vs MUT: * p=0.025 (5'), * p=0.011 (15'), ** p=0.002 (30'), *** p=0.0006 (60'); Two-way ANOVA followed by Bonferroni post-hoc test, n=4) (**Fig. 6D**).

Because AKT signaling is also involved in cell proliferation, we tested the effects of wild-type and mutated SEMA3G on GN11 cell proliferation. For this experiment, GN11 cells were serum-starved overnight and then treated with control, wild-type or mutated SEMA3G concentrated CM, for 24h. We found that SEMA3G induced an increase of approximately 50% in the proliferation of GN11 cells, measured by counting the number of PHH3^{+} cells, compared to control. Instead, SEMA3G^{G166V} was less effective in promoting GN11 cell proliferation (**Fig. 6E**; PHH3^{+} cells/field ± s.e.m.; control CM 9.2±0.5; wild-type SEMA3G 18.3±1.5; SEMA3G^{G166V} 7.0±0.5; ** p=0.001 (control CM vs wild-type SEMA3G), p=0.294 (control CM vs SEMA3G^{G166V}), *** p=0.0003 (wild-type SEMA3G vs SEMA3G^{G166V}); One-way ANOVA followed by Tuckey post-hoc test, n=3). Taken together, these observations suggested that SEMA3G activated AKT signaling and promoted migration and proliferation of immature GnRH neurons, whilst the SEMA3G^{G166V} mutation interfered with these

functions.

Based on findings in the genetic *Sema3g*-null mouse model, combined with the identification of a *SEMA3G* mutation in two brothers with HH and our tissue culture studies using recombinant wild-type and mutated SEMA3G, we demonstrated that SEMA3G may act physiologically to control GnRH neuron development, but its role is redundant in adulthood. Yet, mutated SEMA3G may interfere with other PLXNA-dependent signaling pathways to indirectly cause GnRH deficiency, including HH.

DISCUSSION

Here, we identified two brothers born from consanguineous parents who were affected by a novel syndrome characterized by reproductive defects, facial dysmorphic features and developmental delay.

Both brothers showed cryptorchidism during infancy and absence of response to GnRH stimulation test in early childhood, which can be both suggestive of HH (4). Further, although the hCG test performed in early childhood was normal, there are evidences showing that 50% of boys with HH and cryptorchidism showed a normal testosterone response to hCG stimulation and that hCG can be used in pediatric practice as a treatment for boys with HH (59–64). An HH diagnosis was therefore suspected and confirmed for the older brother who presented at 15 years with typical settings of hypogonadal testes and hormonal levels (testosterone and gonadotropins).

Based on the pattern of inheritance of this disorder, the composition of the family trio with unaffected and affected siblings and the consanguineous marriage, we hypothesized an autosomal recessive syndrome. Thus, by combining HZM with exome sequencing and filtering strategies we identified a mutation in the *SEMA3G* gene within the shared homozygous region on chromosome 3. Because HH is the major feature of our probands and class 3 semaphorins play essential roles in

GnRH neuron development and, when mutated, can cause HH/KS (9,10,12,13), we performed expression and functional experiments to study the possible role of Sema3g in the GnRH system. We found that *Sema3g* mRNA is expressed in the nasal compartment with a spatial and temporal pattern similar to other class 3 semaphorins and their receptors (e.g Sema3a, Nrp1-2) (9,11). In agreement with previous reports showing *Sema3g* expression on BV (17,19), *Sema3g*$^{+}$ cells navigating in the nasal parenchyma are endothelial cells, which have been previously proposed to form a neurovascular niche along migrating GnRH neurons (24,65). Interestingly, a recent paper has shown that endothelial Sema3g regulates synaptic plasticity in the brain (19), strongly supporting a role for this molecule as interplay between vascular and nervous systems.

Our expression studies also highlighted *Sema3g* expression in the developing pituitary gland and hypothalamus, which represent additional key players in the HPG axis that control reproduction.

Because the patients carried homozygous mutations of *SEMA3G*, at first instance we analyzed homozygous *Sema3g*-null mice to model human mutation and functionally study the requirement of Sema3g in the development of the GnRH system. We found a decreased number of GnRH neurons reaching the FB of *Sema3g*-null mice compared to wild-types during embryonic development. Yet, *Sema3g*$^{-/-}$ adult brains contained a normal number of neurons in the MPOA and exhibited an equally innervated ME. In line with these results, no gross alterations were found in testes morphology or in the terminal differentiation of pituitary cells. Although a moderate decrease in *α-GSU*$^{+}$ gonadotrophs and *Pit-1*-independent thyrotrophs during development, these changes are likely due to a developmental delay in lineage differentiation.

Phenotypic differences between embryonic and adult stages might be explained by redundant signaling of semaphorins and their receptors/co-receptors (66), whose lack *in vivo* could be compensated by other members of the family controlling GnRH neuron migration. In agreement, *Sema4d*- and *Gnrh1Cre;Itgb1*$^{fl/fl}$-null mice show a defective GnRH neuron development, but present

a normal HPG axis in adulthood (67,68).

Further, given the nature of the mutation, which is predicted to cause receptor binding alterations, homozygous *Sema3g*-null mice may not represent the optimal model to functionally validate the mutation pathogenicity. With advances in genome editing, it would be interesting to confirm our *in silico* and *in vitro* results by generating a knock-in mouse carrying the SEMA3G mutation at the homologous human position (69).

The increased stability of SEMA3G^{G166V}-PLXNA1 complex is also in line with our *in vitro* experiments on COS-7 cells, in which the mutation induces increased binding to PLXNA1 receptor compared to wild-type SEMA3G, and on immortalized GnRH neurons, which express both PLXNA4 and PLXNA1 receptors. The latter experiments revealed that mutated SEMA3G is less effective in promoting migration, proliferation and AKT activation, compared to wild-type. This could be due to PLXNA1 binding by mutant SEMA3G with a higher affinity than the wild-type counterpart, leading to reduced ligand availability to bind its canonical co-receptor PLXNA4 and to promote GN11 migration. Alternatively, the increased affinity of mutant SEMA3G for PLXNA1 might induce a downstream signaling cascade that acts by suppressing PLXNA4-promoted neuronal migration, proliferation and AKT activation. Interestingly, PLXNA1, which in mouse mediates Sema3a-dependent VN patterning in the nose, can be mutated in patients with HH (11). Thus, *in vivo,* mutated SEMA3G might interfere with the SEMA3A/PLXNA1 signaling in the nose, and indirectly cause HH. Accordingly, our competitive binding assays with mutant SEMA3G and wild-type SEMA3A on tissues and GN11 cells support this hypothesis, as revealed by the less effective binding of SEMA3A on tissues pre-absorbed with mutant 3G and by the reduced response of GN11 cells to SEMA3A when co-exposed to mutant SEMA3G.

In conclusion, we have identified two brothers born from consanguineous parents and affected by a novel syndrome characterized by HH, facial dysmorphic features and intellectual disabilities. By combining homozygosity mapping with exome sequencing, *in silico*, *in vitro* and *in*

vivo mouse models, we provided evidence that SEMA3G affects GnRH neuron development and altered SEMA3G signaling might indirectly cause HH.

Finally, given the complexity of this disease and the nature of the mutation, further genetic and functional studies will be necessary to understand if the phenotypic spectrum of the patients might arise from additional mutated genes and if similar mutations may be found in unrelated patients.

Acknowledgements

We would like to thank Kerra Pearce from University College London (UCL) Genomics Centre at the UCL Great Ormond Street Institute of Child Health for performing homozygosity mapping. We thank Dr F. Memi for the *Gnrh* riboprobe, Dr W. Andrews for hPLXNA1/A4 plasmids and Dr M. Wegner for the anti-Sox9 antibody.

We thank Carleen Spegg, Stella Hertel and Matteo Paxia for technical assistance and the staff of the DKFZ Laboratory Animal Facility for their excellent support with mouse husbandry. Part of this work was carried out at NOLIMITS, an advanced imaging facility established by the Università degli Studi di Milano. We also would like to thank Barbara Boch, Alessandro Fantin and Roberta Azzarelli for critically reading our manuscript.

Statement of Ethics

Ethical approval for the study was granted by UCL Great Ormond Street Institute of Child Health. Informed consent had been taken from the parents for the collection and storage of their DNA samples, along with the samples of their affected and unaffected children who were under the legal age at the time.

Disclosure Statement

The authors have no conflicts of interest to declare.

Funding Sources

A.C. was funded by a grant from the Italian Telethon Foundation [GGP13142] and by the CHARGE Syndrome Foundation. V.A. was partially supported by a Fellowship from Fondazione Veronesi. V.S. and C.G.M. are funded by Action Medical Research (Grant Number GN2272), Barts & The London Charity (BTLC; Grant Number 417/2238) and by Early Career Fellowship from Medical College of Saint Bartholomew's Hospital Trust. DFG CRC1366 "*Vascular Control of Organ Function*"

[project number 39404578]) to H.G.A.

Author Contributions

A.C. designed the experiments, analyzed the data and prepared the manuscript. R.O., V.A., A.L., performed experiments and critically helped with analysis and interpretations of the results. M.V.C, S.G., A.P, V.S., L.D., L.C, F.B. and C.G.M. performed experiments. S.T. and K.H. identified the HH patients with the SEMA3G mutation and performed sequencing and filtering analyses. I.E. and C.P. performed the bioinformatic analyses. L.R. and H.G.A. provided vital samples and ideas.

REFERENCES

1. Herbison AE. Control of puberty onset and fertility by gonadotropin-releasing hormone neurons. Nat Rev Endocrinol [Internet]. 2016 Aug 20;12(8):452–66. Available from: http://www.nature.com/articles/nrendo.2016.70
2. Wierman ME, Kiseljak-Vassiliades K, Tobet S. Gonadotropin-releasing hormone (GnRH) neuron migration: initiation, maintenance and cessation as critical steps to ensure normal reproductive function. Front Neuroendocrinol [Internet]. 2011 Jan;32(1):43–52. Available from: http://www.ncbi.nlm.nih.gov/pubmed/20650288
3. Kim SH. Congenital Hypogonadotropic Hypogonadism and Kallmann Syndrome: Past, Present, and Future. Endocrinol Metab (Seoul, Korea) [Internet]. 2015 Dec;30(4):456–66. Available from: http://dx.doi.org/10.3803/EnM.2015.30.4.456
4. Boehm U, Bouloux P-M, Dattani MT, de Roux N, Dodé C, Dunkel L, et al. Expert consensus document: European Consensus Statement on congenital hypogonadotropic hypogonadism--pathogenesis, diagnosis and treatment. Nat Rev Endocrinol [Internet]. 2015 Sep;11(9):547–64. Available from: http://dx.doi.org/10.1038/nrendo.2015.112
5. Burman P, Ritzén EM, Lindgren AC. Endocrine dysfunction in Prader-Willi syndrome: a review with special reference to GH. Endocr Rev [Internet]. 2001 Dec;22(6):787–99. Available from: http://ovidsp.ovid.com/ovidweb.cgi?T=JS&PAGE=reference&D=emed5&NEWS=N&AN=2002097675
6. Forsythe E, Beales PL. Bardet-Biedl syndrome. Eur J Hum Genet [Internet]. 2013 Jan;21(1):8–13. Available from: http://www.ncbi.nlm.nih.gov/pubmed/22713813
7. Balasubramanian R, Crowley WF. Reproductive endocrine phenotypes relating to CHD7 mutations in humans. Am J Med Genet C Semin Med Genet [Internet]. 2017;175(4):507–15. Available from: http://www.ncbi.nlm.nih.gov/pubmed/29152903
8. Taniguchi M, Masuda T, Fukaya M, Kataoka H, Mishina M, Yaginuma H, et al. Identification and characterization of a novel member of murine semaphorin family. Genes Cells [Internet]. 2005 Aug;10(8):785–92. Available from: http://www.ncbi.nlm.nih.gov/pubmed/16098142
9. Cariboni A, Davidson K, Rakic S, Maggi R, Parnavelas JG, Ruhrberg C. Defective gonadotropin-releasing hormone neuron migration in mice lacking SEMA3A signalling through NRP1 and NRP2: implications for the aetiology of hypogonadotropic hypogonadism. Hum Mol Genet [Internet]. 2011 Jan 15;20(2):336–44. Available from: http://www.ncbi.nlm.nih.gov/pubmed/21059704
10. Cariboni A, André V, Chauvet S, Cassatella D, Davidson K, Caramello A, et al. Dysfunctional SEMA3E signaling underlies gonadotropin-releasing hormone neuron deficiency in Kallmann syndrome. J Clin Invest [Internet]. 2015 Jun 1;125(6):2413–28. Available from: http://www.jci.org/articles/view/78448
11. Marcos S, Monnier C, Rovira X, Fouveaut C, Pitteloud N, Ango F, et al. Defective signaling through plexin-A1 compromises the development of the peripheral olfactory system and neuroendocrine reproductive axis in mice. Hum Mol Genet [Internet]. 2017;26(11):2006–17. Available from: http://www.ncbi.nlm.nih.gov/pubmed/28334861
12. Hanchate NK, Giacobini P, Lhuillier P, Parkash J, Espy C, Fouveaut C, et al. SEMA3A, a gene involved in axonal pathfinding, is mutated in patients with Kallmann syndrome. PLoS Genet [Internet]. 2012 Aug;8(8):e1002896. Available from: http://www.ncbi.nlm.nih.gov/pubmed/22927827
13. Young J, Metay C, Bouligand J, Tou B, Francou B, Maione L, et al. SEMA3A deletion in a family with Kallmann syndrome validates the role of semaphorin 3A in human puberty and olfactory system development. Hum Reprod [Internet]. 2012 May;27(5):1460–5. Available from: http://www.ncbi.nlm.nih.gov/pubmed/22416012
14. Lettieri A, Oleari R, Gimmelli J, ANDRé V, Cariboni A. The role of semaphorin signaling in the etiology of hypogonadotropic hypogonadism. Minerva Endocrinol [Internet]. 2016 Jun;41(2):266–78. Available from: http://www.ncbi.nlm.nih.gov/pubmed/26940457
15. Cariboni A, Oleari R, Lettieri A, Paganoni A, Zanieri L. Semaphorin signalling in GnRH neurons: from development to disease. Neuroendocrinology [Internet]. 2018 Dec 2;30504719. Available from: https://www.karger.com/Article/FullText/495916
16. Kotan LD, Isik E, Turan I, Mengen E, Akkus G, Tastan M, et al. Prevalence and associated phenotypes of PLXNA1 variants in normosmic and anosmic idiopathic hypogonadotropic hypogonadism. Clin

Genet [Internet]. 2019 Feb;95(2):320–4. Available from: http://www.ncbi.nlm.nih.gov/pubmed/30467832
17. Kutschera S, Weber H, Weick A, De Smet F, Genove G, Takemoto M, et al. Differential endothelial transcriptomics identifies semaphorin 3G as a vascular class 3 semaphorin. Arterioscler Thromb Vasc Biol [Internet]. 2011 Jan;31(1):151–9. Available from: http://www.ncbi.nlm.nih.gov/pubmed/20947821
18. Liu X, Uemura A, Fukushima Y, Yoshida Y, Hirashima M. Semaphorin 3G Provides a Repulsive Guidance Cue to Lymphatic Endothelial Cells via Neuropilin-2/PlexinD1. Cell Rep [Internet]. 2016;17(9):2299–311. Available from: http://dx.doi.org/10.1016/j.celrep.2016.11.008
19. Tan C, Lu N-N, Wang C, Chen D, Sun N, Lyu H, et al. Endothelium-Derived Semaphorin 3G Regulates Hippocampal Synaptic Structure and Plasticity via Neuropilin-2/PlexinA4. Neuron [Internet]. 2019 Jan 16;1–18. Available from: https://www.cell.com/neuron/fulltext/S0896-6273(18)31156-5
20. Zhang Y, Chen K, Sloan SA, Bennett ML, Scholze AR, O'Keeffe S, et al. An RNA-sequencing transcriptome and splicing database of glia, neurons, and vascular cells of the cerebral cortex. J Neurosci [Internet]. 2014 Sep 3;34(36):11929–47. Available from: http://www.jneurosci.org/cgi/doi/10.1523/JNEUROSCI.1860-14.2014
21. Dasen JS, Barbera JPM, Herman TS, O'Connell S, Olson L, Ju B, et al. Temporal regulation of a paired-like homeodomain repressor/TLE corepressor complex and a related activator is required for pituitary organogenesis. Genes Dev. 2001;15(23):3193–207.
22. Howard SR, Oleari R, Poliandri A, Chantzara V, Fantin A, Ruiz-Babot G, et al. HS6ST1 insufficiency causes self-limited delayed puberty in contrast with other GnRH deficiency genes. J Clin Endocrinol Metab [Internet]. 2018 Jun 20;117(2):457–63. Available from: https://academic.oup.com/jcem/article/103/9/3420/5040368
23. Oprych K, Cotfas D, Choi D. Common olfactory ensheathing glial markers in the developing human olfactory system. Brain Struct Funct [Internet]. 2017 May;222(4):1877–95. Available from: http://www.ncbi.nlm.nih.gov/pubmed/27718014
24. Cariboni A, Davidson K, Dozio E, Memi F, Schwarz Q, Stossi F, et al. VEGF signalling controls GnRH neuron survival via NRP1 independently of KDR and blood vessels. Development [Internet]. 2011 Sep;138(17):3723–33. Available from: http://dev.biologists.org/cgi/doi/10.1242/dev.063362
25. Gaston-Massuet C, McCabe MJ, Scagliotti V, Young RM, Carreno G, Gregory LC, et al. Transcription factor 7-like 1 is involved in hypothalamo-pituitary axis development in mice and humans. Proc Natl Acad Sci U S A [Internet]. 2016 Feb 2;113(5):E548-57. Available from: http://www.ncbi.nlm.nih.gov/pubmed/26764381
26. Gaston-Massuet C, Andoniadou CL, Signore M, Jayakody SA, Charolidi N, Kyeyune R, et al. Increased Wingless (Wnt) signaling in pituitary progenitor/stem cells gives rise to pituitary tumors in mice and humans. Proc Natl Acad Sci [Internet]. 2011;108(28):11482–7. Available from: http://www.pnas.org/cgi/doi/10.1073/pnas.1101553108
27. Riascos-Bernal DF, Chinnasamy P, Cao L, Dunaway CM, Valenta T, Basler K, et al. β-Catenin C-terminal signals suppress p53 and are essential for artery formation. Nat Commun. 2016;7(7):2–3.
28. Groppa E, Brkic S, Uccelli A, Wirth G, Korpisalo-Pirinen P, Filippova M, et al. EphrinB2/EphB4 signaling regulates non-sprouting angiogenesis by VEGF. EMBO Rep [Internet]. 2018;19(5):e45054. Available from: http://embor.embopress.org/lookup/doi/10.15252/embr.201745054
29. Barrionuevo F, Georg I, Scherthan H, Lécureuil C, Guillou F, Wegner M, et al. Testis cord differentiation after the sex determination stage is independent of Sox9 but fails in the combined absence of Sox9 and Sox8. Dev Biol [Internet]. 2009;327(2):301–12. Available from: http://dx.doi.org/10.1016/j.ydbio.2008.12.011
30. Jokela H, Hakkarainen J, Kätkänaho L, Pakarinen P, Ruohonen ST, Tena-Sempere M, et al. Deleting the mouse Hsd17b1 gene results in a hypomorphic Naglu allele and a phenotype mimicking a lysosomal storage disease. Sci Rep [Internet]. 2017 Nov 27;7(1):16406. Available from: http://www.ncbi.nlm.nih.gov/pubmed/29180785
31. Memi F, Abe P, Cariboni A, MacKay F, Parnavelas JG, Stumm R. CXC chemokine receptor 7 (CXCR7) affects the migration of GnRH neurons by regulating CXCL12 availability. J Neurosci [Internet]. 2013 Oct 30;33(44):17527–37. Available from: http://www.jneurosci.org/cgi/doi/10.1523/JNEUROSCI.0857-13.2013

32. Busnelli M, Manzini S, Hilvo M, Parolini C, Ganzetti GS, Dellera F, et al. Liver-specific deletion of the Plpp3 gene alters plasma lipid composition and worsens atherosclerosis in apoE -/- mice. Sci Rep. 2017;7(November 2016):1–13.
33. Janssen BJC, Robinson RA, Pérez-Brangulí F, Bell CH, Mitchell KJ, Siebold C, et al. Structural basis of semaphorin-plexin signalling. Nature [Internet]. 2010 Oct 28;467(7319):1118–22. Available from: http://www.ncbi.nlm.nih.gov/pubmed/20877282
34. Radovick S, Wray S, Lee E, Nicols DK, Nakayama Y, Weintraub BD, et al. Migratory arrest of gonadotropin-releasing hormone neurons in transgenic mice. Proc Natl Acad Sci U S A [Internet]. 1991 Apr 15;88(8):3402–6. Available from: http://www.ncbi.nlm.nih.gov/pubmed/2014260
35. Cariboni A, Pimpinelli F, Colamarino S, Zaninetti R, Piccolella M, Rumio C, et al. The product of X-linked Kallmann's syndrome gene (KAL1) affects the migratory activity of gonadotropin-releasing hormone (GnRH)-producing neurons. Hum Mol Genet [Internet]. 2004 Nov 15;13(22):2781–91. Available from: http://www.ncbi.nlm.nih.gov/pubmed/15471890
36. Cynthia C, Berger B. Laboratory Tests and Diagnostic Procedures - 6th Edition. 6th ed. Saunders; 2012. 1059–1062 p.
37. Barraud S, Delemer B, Poirsier-Violle C, Bouligand J, Mérol J-C, Grange F, et al. Congenital hypogonadotropic hypogonadism with anosmia and Gorlin features caused by a PTCH1 mutation reveals a new candidate gene for Kallmann syndrome. Neuroendocrinology [Internet]. 2020 Feb 20; Available from: http://www.ncbi.nlm.nih.gov/pubmed/32074614
38. Löfqvist C, Andersson E, Gelander L, Rosberg S, Blum WF, Albertsson Wikland K. Reference values for IGF-I throughout childhood and adolescence: a model that accounts simultaneously for the effect of gender, age, and puberty. J Clin Endocrinol Metab [Internet]. 2001 Dec;86(12):5870–6. Available from: http://www.ncbi.nlm.nih.gov/pubmed/11739455
39. Adzhubei IA, Schmidt S, Peshkin L, Ramensky VE, Gerasimova A, Bork P, et al. A method and server for predicting damaging missense mutations. Nat Methods [Internet]. 2010 Apr;7(4):248–9. Available from: http://www.ncbi.nlm.nih.gov/pubmed/20354512
40. Ng PC, Henikoff S. SIFT: Predicting amino acid changes that affect protein function. Nucleic Acids Res [Internet]. 2003 Jul 1;31(13):3812–4. Available from: http://www.ncbi.nlm.nih.gov/pubmed/12824425
41. Schwarz JM, Cooper DN, Schuelke M, Seelow D. MutationTaster2: mutation prediction for the deep-sequencing age. Nat Methods [Internet]. 2014 Apr;11(4):361–2. Available from: http://dx.doi.org/10.1038/nmeth.2890
42. Wray S. From nose to brain: development of gonadotrophin-releasing hormone-1 neurones. J Neuroendocrinol [Internet]. 2010 Jul;22(7):743–53. Available from: http://www.pubmedcentral.nih.gov/articlerender.fcgi?artid=2919238&tool=pmcentrez&rendertype=abstract
43. Miller AM, Treloar HB, Greer CA. Composition of the migratory mass during development of the olfactory nerve. J Comp Neurol [Internet]. 2010 Dec 15;518(24):4825–41. Available from: http://www.ncbi.nlm.nih.gov/pubmed/21031554
44. Teshima THN, Wells KL, Lourenço S V, Tucker AS. Apoptosis in Early Salivary Gland Duct Morphogenesis and Lumen Formation. J Dent Res [Internet]. 2016 Mar;95(3):277–83. Available from: http://www.ncbi.nlm.nih.gov/pubmed/26628486
45. Bodner M, Castrillo JL, Theill LE, Deerinck T, Ellisman M, Karin M. The pituitary-specific transcription factor GHF-1 is a homeobox-containing protein. Cell [Internet]. 1988 Nov 4;55(3):505–18. Available from: http://www.ncbi.nlm.nih.gov/pubmed/2902927
46. Camper SA, Saunders TL, Katz RW, Reeves RH. The Pit-1 transcription factor gene is a candidate for the murine Snell dwarf mutation. Genomics. 1990;8(3):586–90.
47. Ingraham HA, Lala DS, Ikeda Y, Luo X, Shen WH, Nachtigal MW, et al. The nuclear receptor steroidogenic factor 1 acts at multiple levels of the reproductive axis. Genes Dev. 1994;8(19):2302–12.
48. Lamolet B, Pulichino AM, Lamonerie T, Gauthier Y, Brue T, Enjalbert A, et al. A pituitary cell-restricted T box factor, Tpit, activates POMC transcription in cooperation with Pitx homeoproteins. Cell. 2001;104(6):849–59.
49. Pulichino AM, Vallette-Kasic S, Tsai JPY, Couture C, Gauthier Y, Drouin J. Tpit determines alternate

fates during pituitary cell differentiation. Genes Dev. 2003;17(6):738–47.
50. Pierce JG, Parsons TF. Glycoprotein Hormones: Structure and Function. Annu Rev Biochem [Internet]. 1981;50(1):465–95. Available from: http://www.annualreviews.org/doi/10.1146/annurev.bi.50.070181.002341
51. Bhattacharya A, Wunderlich Z, Monleon D, Tejero R, Montelione GT. Assessing model accuracy using the homology modeling automatically (HOMA) software. Proteins Struct Funct Genet. 2008;70(1):105–18.
52. Forrest LR, Tang CL, Honig B. On the accuracy of homology modeling and sequence alignment methods applied to membrane proteins. Biophys J. 2006;91(2):508–17.
53. Zhang Z, Wang L, Gao Y, Zhang J, Zhenirovskyy M, Alexov E. Predicting folding free energy changes upon single point mutations. Bioinformatics [Internet]. 2012 Mar 1;28(5):664–71. Available from: http://www.ncbi.nlm.nih.gov/pubmed/22238268
54. Dehouck Y, Grosfils A, Folch B, Gilis D, Bogaerts P, Rooman M. Fast and accurate predictions of protein stability changes upon mutations using statistical potentials and neural networks: PoPMuSiC-2.0. Bioinformatics. 2009;25(19):2537–43.
55. Im W, Feig M, Brooks CL. An implicit membrane generalized born theory for the study of structure, stability, and interactions of membrane proteins. Biophys J [Internet]. 2003 Nov;85(5):2900–18. Available from: file:///scielo.php?script=sci_arttext&pid=S1726-22162009000100012&lang=pt
56. Andrews WD, Barber M, Nemitz M, Memi F, Parnavelas JG. Semaphorin3A-neuropilin1 signalling is involved in the generation of cortical interneurons. Brain Struct Funct [Internet]. 2017 Jul;222(5):2217–33. Available from: http://www.ncbi.nlm.nih.gov/pubmed/27858201
57. Cariboni A, Hickok J, Rakic S, Andrews W, Maggi R, Tischkau S, et al. Neuropilins and their ligands are important in the migration of gonadotropin-releasing hormone neurons. J Neurosci [Internet]. 2007 Feb 28;27(9):2387–95. Available from: http://www.jneurosci.org/cgi/doi/10.1523/JNEUROSCI.5075-06.2007
58. Magni P, Dozio E, Ruscica M, Watanobe H, Cariboni A, Zaninetti R, et al. Leukemia inhibitory factor induces the chemomigration of immortalized gonadotropin-releasing hormone neurons through the independent activation of the Janus kinase/signal transducer and activator of transcription 3, mitogen-activated protein kinase/extrac. Mol Endocrinol [Internet]. 2007 May;21(5):1163–74. Available from: http://www.ncbi.nlm.nih.gov/pubmed/17299136
59. Vicari E, Mongioì A, Calogero AE, Moncada ML, Sidoti G, Polosa P, et al. Therapy with human chorionic gonadotrophin alone induces spermatogenesis in men with isolated hypogonadotrophic hypogonadism-long-term follow-up. Int J Androl. 1992;15(4):320–9.
60. Kung AW, Zhong YY, Lam KS, Wang C. Induction of spermatogenesis with gonadotrophins in Chinese men with hypogonadotrophic hypogonadism. Int J Androl [Internet]. 1994 Oct;17(5):241–7. Available from: http://www.ncbi.nlm.nih.gov/pubmed/7698849
61. Raivio T, Toppari J, Perheentupa A, McNeilly AS, Dunkel L. Treatment of prepubertal gonadotrophin-deficient boys with recombinant human follicle-stimulating hormone. Lancet (London, England) [Internet]. 1997 Jul 26;350(9073):263–4. Available from: http://www.ncbi.nlm.nih.gov/pubmed/9242808
62. Burris AS, Rodbard HW, Winters SJ, Sherins RJ. Gonadotropin therapy in men with isolated hypogonadotropic hypogonadism: the response to human chorionic gonadotropin is predicted by initial testicular size. J Clin Endocrinol Metab [Internet]. 1988 Jun;66(6):1144–51. Available from: http://www.ncbi.nlm.nih.gov/pubmed/3372679
63. Tamunopriye J, Abiola OO. Human chorionic gonadotrophin (HCG) stimulation test and testosterone response in children with micropenis. Pediatr Endocrinol Rev [Internet]. 2014 Sep;12(1):42–5. Available from: http://www.ncbi.nlm.nih.gov/pubmed/25345084
64. Rohayem J, Hauffa BP, Zacharin M, Kliesch S, Zitzmann M, "German Adolescent Hypogonadotropic Hypogonadism Study Group." Testicular growth and spermatogenesis: new goals for pubertal hormone replacement in boys with hypogonadotropic hypogonadism? -a multicentre prospective study of hCG/rFSH treatment outcomes during adolescence. Clin Endocrinol (Oxf) [Internet]. 2017 Jan;86(1):75–87. Available from: http://www.ncbi.nlm.nih.gov/pubmed/27467188
65. Saghatelyan A. Role of blood vessels in the neuronal migration. Semin Cell Dev Biol. 2009;20(6):744–50.

66. Sharma A, Verhaagen J, Harvey AR. Receptor complexes for each of the Class 3 Semaphorins. Front Cell Neurosci [Internet]. 2012;6(July):28. Available from: http://journal.frontiersin.org/article/10.3389/fncel.2012.00028/abstract
67. Giacobini P, Messina A, Morello F, Ferraris N, Corso S, Penachioni J, et al. Semaphorin 4D regulates gonadotropin hormone-releasing hormone-1 neuronal migration through PlexinB1-Met complex. J Cell Biol [Internet]. 2008 Nov 3;183(3):555–66. Available from: http://www.ncbi.nlm.nih.gov/pubmed/18981235
68. Parkash J, Cimino I, Ferraris N, Casoni F, Wray S, Cappy H, et al. Suppression of β1-integrin in gonadotropin-releasing hormone cells disrupts migration and axonal extension resulting in severe reproductive alterations. J Neurosci [Internet]. 2012 Nov 21;32(47):16992–7002. Available from: https://www.ncbi.nlm.nih.gov/pmc/articles/PMC4485391/
69. Hara S, Takada S. Genome editing for the reproduction and remedy of human diseases in mice. J Hum Genet. 2018;63(2):107–13.

FIGURES LEGENDS

Figure 1. Homozygosity mapping identifies a *SEMA3G* mutation in two brothers affected by reproductive defects, dysmorphic features and developmental delay.

(A) Pedigree of the affected brothers. Circle denotes female; square denotes male; black square denotes affected male. **(B)** The panel shows a B-allele frequency plot of chromosome 3, with heterozygous SNPs plotted at 0.5, and homozygous SNPs plotted at either position 0 or 1. Highlighted in green are the homozygous regions. As seen from the image, a large region spanning base pair positions 27663546 to 65514406 (approximately 38 Mb) is shared between the two affected patients. This homozygous region is absent in the unaffected siblings. A small homozygous region of 1.3 Mb is also presented in the figure. This represents the largest shared homozygous region on chromosome 3. **(C)** Chromatograms of nucleotides 492 to 501 of the *SEMA3G* coding sequence from 2 brothers carrying a nucleotide substitution in exon 5 (left side, forward strand; right side, reverse strand; the positions of the G>T and corresponding C>A change are indicated with asterisks) and from the unaffected parents and sisters. **(D)** *In silico* analysis identified *SEMA3G* on chromosome 3 as a potential candidate gene, with nucleotide change c.497G>T and protein change p.Gly166Val. PolyPhen-2, SIFT and Mutation Taster were used to predict structural and functional effects of p.G166V amino acid substitution on SEMA3G protein structure and function. The mutation was predicted to be possibly damaging (Poly-Phen), damaging (SIFT) and disease causing (Mutation Taster) with probabilistic scores above 0.99. **(E)** Diagram of the SEMA3G functional domains: SEMA and Ig-like. Their position and the position of the mutated amino acid residue within the protein sequence are indicated. **(F)** Genomic evolutionary rate profiling of sequence constraint for the SEMA3G mutation in the 2 brothers using GERP++ analysis provided an RS score of 3.79, which is close to the maximum score of 6.18 for complete conservation across all mammalian species. (**G**) Alignment of partial protein sequences of vertebrate SEMA3G orthologues shows that the G166 residue is evolutionarily conserved in humans and several other vertebrate species.

Figure 2. *Sema3g* mRNA expression during GnRH neuron and pituitary development.

(**A-D**) *Sema3g* ISH (green signal) of coronal sections from E13.5 heads at the level of the nasal region followed by immunolabelling (red) for GnRH (**A**) or Tuj1 (**B**) or S100 (**C**) or IB4 (**D**) revealed that *Sema3g* is expressed by cells in close apposition to GnRH neurons, Tuj1^{+}-olfactory neurons and to S100^{+} OECs (white arrows). White arrowheads indicate examples of Sema3g^{+} cells co-expressing endothelial marker IB4. (**E-I**) *Sema3g* ISH on sagittal (**E-H**) and frontal (**I**) histological sections of wild-type pituitaries using antisense riboprobes against *Sema3g*. (**E'**-**I')** are magnified images of the squared areas in A-E, respectively. (**E-E'**) At E10.5, weak staining for *Sema3g* is observed in some cells of the Rathke's pouch, which is the primordium of the pituitary gland, and the ventral diencephalon. (**F-F'**) At E12.5, a peak in *Sema3g* mRNA expression is observed in the rostral and the ventral part of the developing anterior lobe of the pituitary gland (arrowhead). Positive

staining is also detected in the developing hypothalamus (arrows). (**G-G'**) At E14.5, expression is observed in the hypothalamus (arrows) and in some cells scattered throughout the developing anterior pituitary. (**H-H'**) At E15.5, *Sema3g* expression is found only in a few cells of the anterior lobe of the pituitary gland and it becomes almost undetectable at E18.5 (**I-I'**)**.** Abbreviations: VD, ventral diencephalon; RP, Rathke's pouch; HYP, hypothalamus; AL, anterior lobe; INF, infundibulum; PL, posterior lobe; IL, intermediate lobe. Scale bars: 200 µm (**A-D**, low magnifications), 50 µm (**A-D,** high magnifications).: 200 µm (**E-H**), 100 µm (**E'-I'**)**.**
Abbreviations: OE, olfactory epithelium; VNO, vomeronasal organ; NFJ, nasal forebrain junction.

Figure 3. *Sema3g*-null embryos display developmental defects in GnRH neuron migration and pituitary cell lineage.

(A) Coronal sections of wild-type and *Sema3g*-null embryo heads at E14.5 were immunolabelled for GnRH to reveal GnRH neurons in the nasal compartment (panels in first column), in the NFJ (panels in second column) and in the MPOA (panels in third column). Black dots indicate border with OB. Black arrowheads indicate examples of migrating GnRH neurons in the nose, black arrows indicate examples of neurons crossing the OBs. Migrating GnRH neurons in the FB are indicated with black arrowhead while lack of GnRH neurons in the FB of mutants is indicated with Δ. (**B**) Quantitative counting analysis (expressed as mean ± s.e.m) showing a significant reduction in the total number of GnRH neurons in *Sema3g*-deficient mouse heads at E14.5, which is explained by a significant reduction of GnRH neurons reaching the FB (* p=0.017, ** p=0.00**4**; n=3 for each group, two-sided unpaired Student's *t* test). **(C)** ISH on sagittal histological sections of wild-type and *Sema3g*$^{-/-}$ embryos at E14.5 revealed a mild delay in *Pit-1* lineage specification in knockout embryos compared to wild-types (black arrowheads). A modest reduction in *α-GSU* and *Pomc1* mRNA levels is also detected in *Sema3g*$^{-/-}$ embryos (black arrowheads**)**.
Abbreviations: OB, olfactory bulb; OE, olfactory epithelium; VNO, vomeronasal organ; NFJ, nasal forebrain junction; MPOA, medial preoptic area; FB, forebrain; AL, anterior lobe; PL, posterior lobe; MZ, marginal zone; α-GSU, alpha-subunit glycoprotein; Pit-1, pituitary-specific positive transcription factor 1; Pomc1, pro-opiomelanocortin 1. Scale bars: 200 µm.

Figure 4. Sema3g loss does not impair the adult HPG axis.

(A) Coronal sections of adult hypothalamus (P80) of the indicated genotypes at the level of the MPOA (upper panels) and at the level of the ME (lower panels) were immunostained to identify GnRH-positive neurons and axons; examples of normally projecting neurons in the MPOA are indicated with black arrowheads. Innervation of ME was similar between wild-types and mutants. **(B)** Quantification (mean ± s.e.m.) of GnRH neuron numbers in the MPOA and ME innervation of *Sema3g*$^{+/+}$ and *Sema3g*$^{-/-}$ P80 mice (MPOA p=0.315 and ME p=0.195; n=4 for each group, two-sided unpaired Student's *t* test). **(C)** Immunohistochemistry stainings against hormone-producing cells in coronal sections from the pituitaries of the indicated genotypes revealed no differences in terminal differentiation of hormone producing cells between wild-types and mutants. **(D)**

Microtome sections of the indicated genotypes were stained with Hematoxylin and eosin (H&E) (upper panels), for the Sertoli cell marker Sox9 (middle panels) or for the Leydig cell marker Cyp17a1 (lower panels). No differences were observed between wild-types and mutants. Black and white arrowheads indicate examples of normally Sox9 and Cyp17a1 expressing cells, respectively. Nuclei were counterstained with DAPI. **(E)** Quantitative qPCR for *Sox9* and *Cyp17a1* revealed no changes in their expression levels between control and mutant testes (Cyp17a1 mean ± s.e.m.: *Sema3g*$^{+/+}$ 0.9 ± 0.1; *Sema3g*$^{-/-}$ 0.8 ± 0.3, p=0.58**0**; Sox9 mean ± s.e.m.: *Sema3g*$^{+/+}$ 1.0 ± 0.03; *Sema3g*$^{-/-}$ 0.9 ± 0.2, p=0.482; n=3 for each group, two-sided unpaired Student's *t* test).

Abbreviations: MPOA, medial preoptic area; ME, median eminence; 3v, third ventricle; ACTH, adrenocorticotropic hormone, GH, growth hormone, LH, luteinising hormone, PRL, prolactin; TSH, thyroid-stimulating hormone; AL, anterior lobe; IL, intermediate lobe; PL, posterior lobe. Scale bar: 200 µm (A, C), 100 µm (D).

Figure 5. Mutated SEMA3G alters PLXNA binding properties in silico, in vitro and ex vivo.

(A) Interaction network (upper panels) and patch analysis (lower panels) of SEMA3G::PLXNA1 wild-type and mutated SEMA3GG166V::PLXNA1 complexes: Asp410 residue of PLXNA1 (grey ribbons) interacts with Arg167 of both wild-type SEMA3G (yellow ribbons) and p.G166V mutant SEMA3G (orange ribbon). Backbone and side chains are shown in stick representation; atoms involved in ionic and hydrogen bonds are surrounded by blue and red shells, respectively. Wild-type complex. Mild polar and H-Bonding areas on PLXNA1 molecular surface are highlighted in steel blue and purple, respectively (lower panels). Positive charged patch is colored in solid blue and pointed out by arrows; in solid red and arrows is shown positive, unfavourable, ΔG of solvation contribution to the complex formation. **(B,C)** Transfected COS-7 cells express similar levels of wild-type and mutated (SEMA3GG166V) AP-fused human SEMA3G, as revealed by immunofluorescence (B) and immunoblotting (**C**). WB analysis on conditioned media also showed that the p.G166V mutation did not alter protein secretion. (**D**) AP-binding assay on COS-7 cells expressing human PLXNA4 or PLXNA1 after incubation with CM containing AP-conjugated control, wild-type SEMA3G or mutated SEMA3G. The p.G166V mutation increased the binding affinity to PLXNA4 and PLXNA1, as shown by relative quantification of integrated density (SEMA3G^{G166V} vs wild-type SEMA3G: 3.3±0.8 PLXNA4, *p=0.038; PLXNA1 5.6±1.0, **p=0.004; n=4 for wild-type SEMA3G; n=3 for SEMA3G^{G166V}; two-sided unpaired Student's t test. (**E**) Coronal sections of E14.5 mouse heads at the nasal level (nose) or at the forebrain (brain) level were incubated with SEMA3A-AP ligand alone (left panels) or before pre-incubation with SEMA3GG166V-AP ligand (right panels). Arrowheads indicate areas where SEMA3A binds in the nose and in the brain. Delta symbols indicate areas of reduced SEMA3A binding when the tissue was pre-incubated with SEMA3GG166V. Scale bar: 50 µm (**B-D**), 200 µm (**E**).

Figure 6. Mutated SEMA3G protein affects GN11 cell behavior and response to SEMA3A. (A) RT-PCR analysis performed on mRNA extracted from GN11 cells showed the presence of specific transcripts for *Nrp1*, *Nrp2*, *Plxna1*-4 and the standard *Gapdh* with amplicons of 188, 260, 250, 485, 195, 295 and 189 bp, respectively **(B)** AP-binding assay on GN11 cells after incubation with CM containing equal amounts of CTRL, wild-type SEMA3G or mutated SEMA3G. The p.G166V mutation did not affect the binding of SEMA3G on GN11 cells **(C)** Chemotactic response of GN11 cells to wild-type and mutated SEMA3G CM in a Boyden's chamber assay in the absence or presence of SEMA3A. Left graph**:** wild-type SEMA3G induced a significant increase in the chemomigration of GN11 cells compared to control-CM, whereas no statistically significant differences were observed between control-CM and SEMA3G^{G166V}-CM (CTRL vs WT ** p=0.003; CTRL vs G166V p=0.251; WT vs G166V p=0.085; One-way ANOVA followed by Dunnett post-hoc test, n=7). Right graph: wild-type SEMA3A induced a significant decrease in the chemomigration of GN11 cells compared to control-CM; this effect was abolished only when GN11 cells were co-exposed to SEMA3G^{G166V}-CM, but not to SEMA3G-CM (CTRL vs 3A * p=0.011; CTRL vs 3A+3G WT * p=0.011; CTRL vs 3A+3G G166V p=0.808; 3A vs 3A+3G G166V * p=0.035; 3A+3G WT vs 3A+3G G166V * p=0.038; One-way ANOVA followed by Tukey post-hoc test, n=3). **(D)** Representative immunoblots and relative quantification show decreased levels of pAKT, relative to total AKT, in serum-starved GN11 cells treated with mutated SEMA3G protein at each time point (WT vs MUT: * p=0.025 (5'), * p=0.011 (15'), ** p=0.002 (30'), *** p=0.0006 (60'), Two-way ANOVA followed by Tuckey post-hoc test). **(E)** Evaluation of GN11 proliferation by PHH3 immunostaining after 24h incubation with wild-type and mutated SEMA3G CM. Mutated SEMA3G failed to promote cell proliferation compared to wild-type SEMA3G (** p=0.0011, control CM vs wild-type SEMA3G; p=0.294, control CM vs SEMA3G^{G166V}; *** p=0.0003, wild-type SEMA3G vs SEMA3G^{G166V}; One-way ANOVA followed by Tuckey post-hoc test). Data reported in C are shown as relative fold-change ± s.e.m. of n=7 independent experiments. Data reported in D and E are shown as mean ± s.e.m. of n=3 independent experiments. Scale bars: 100 µm (B, E).

A

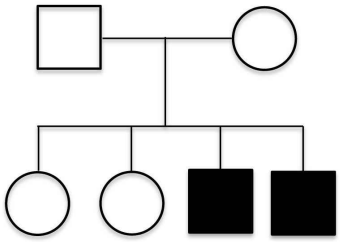

B

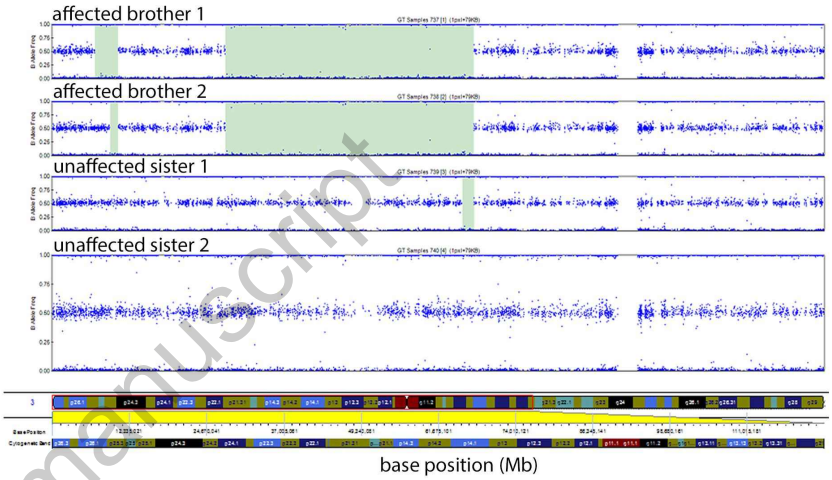

C

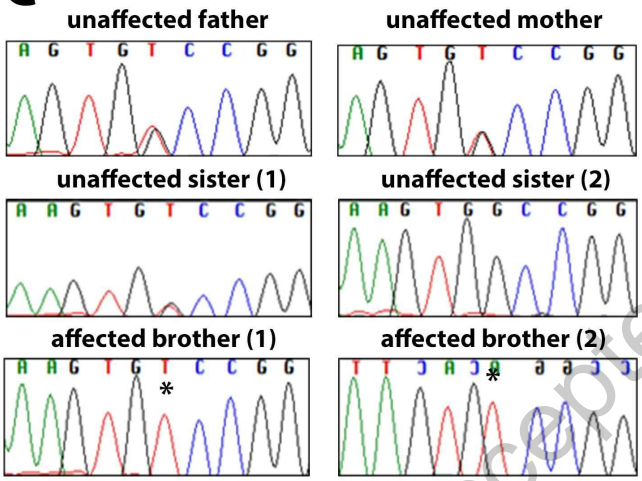

D

Chr	Position	nt sub	aa sub	Poly-Phen	SIFT	Mutation Taster
3	52475888	G>T	G166V	possibly damaging	damaging	disease causing

E

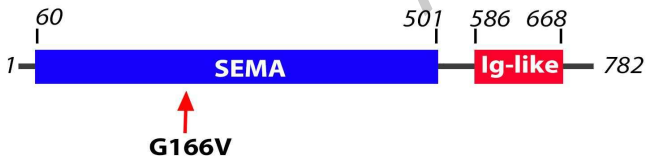

F

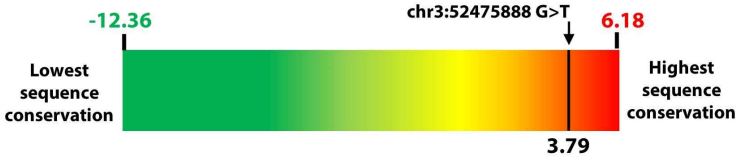

G

166-VLHLEPGSVESGRGR *H. sapiens*
166-VLHLEPGSVESVRGR *H. sapiens* mutated
166-VLRLDASSVENGRGR *M. musculus*
166-VLHLEPGSVESGRGR *P. troglodytes*
55-AFSLDPGSTESGRGR *G. gallus*
158-VFSLDQTTVQNGRGR *D. rerio*

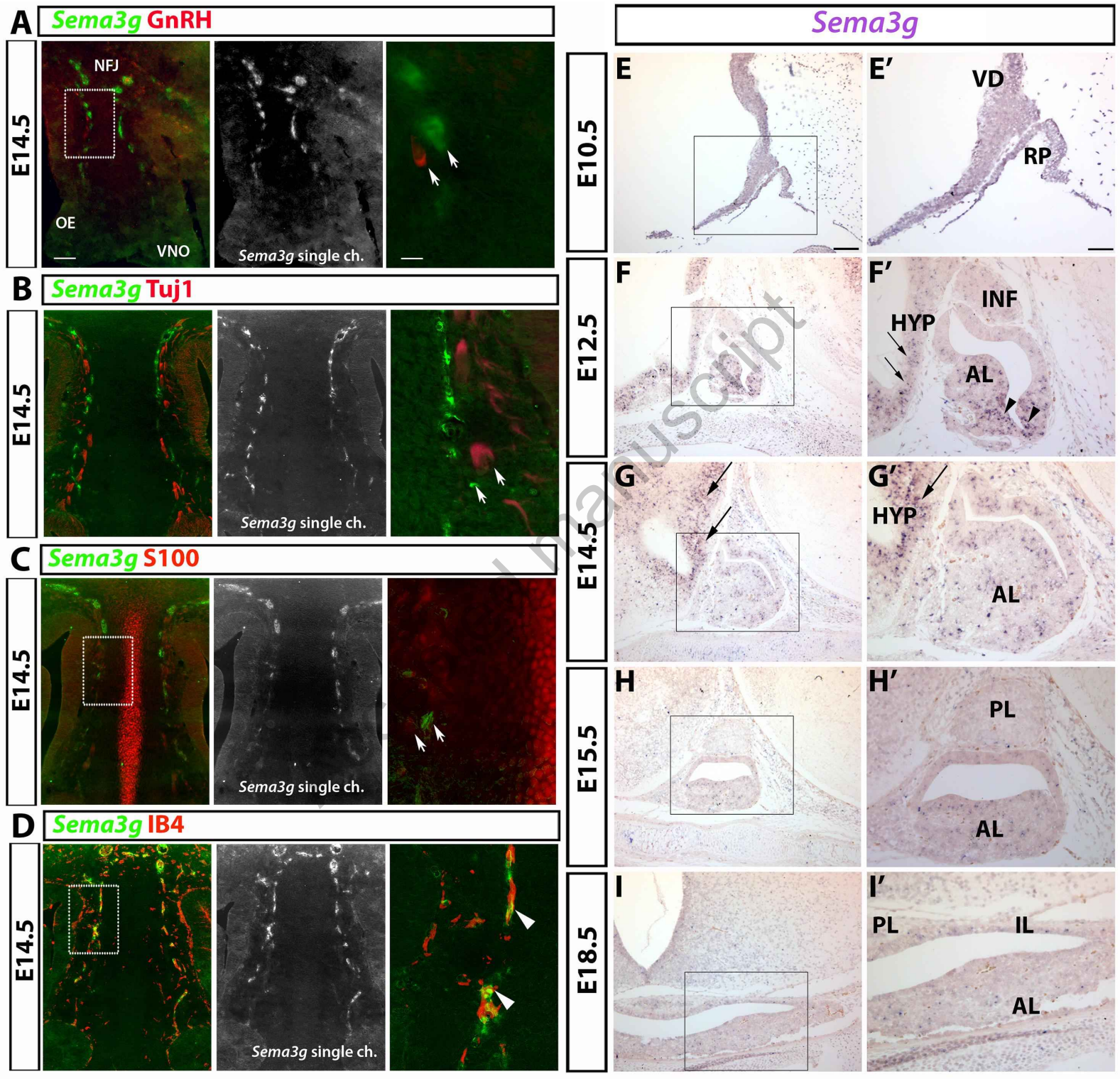

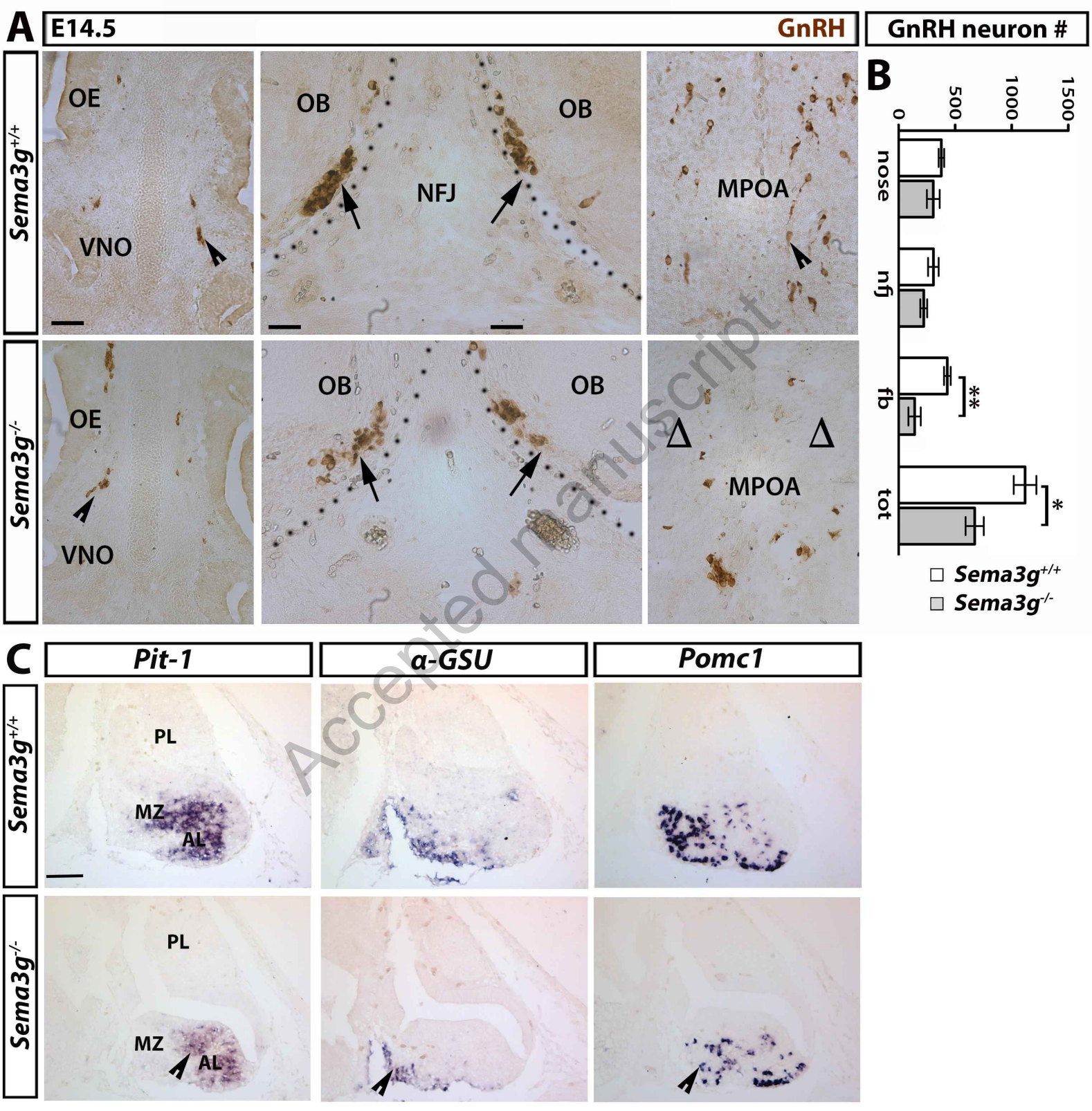

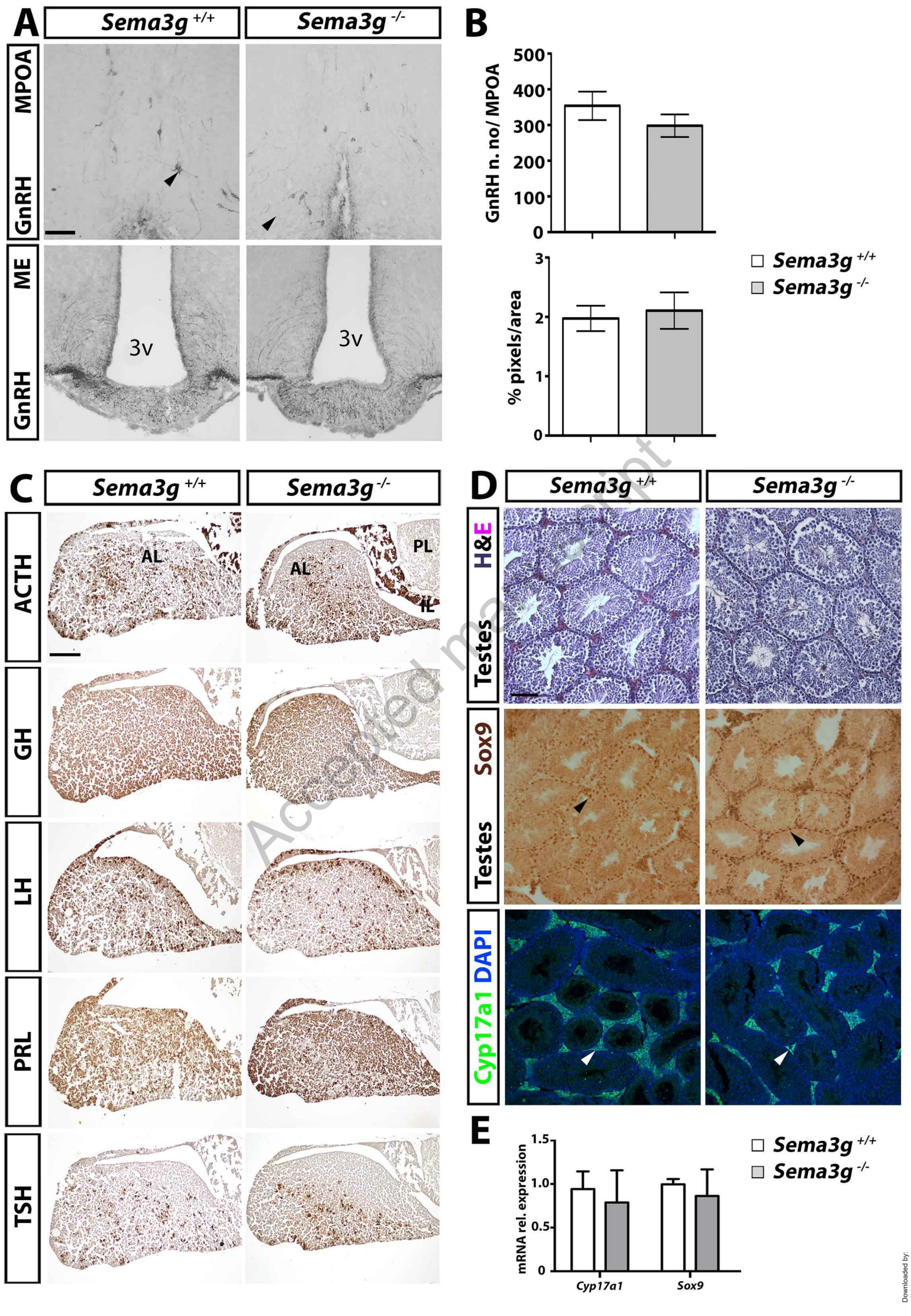

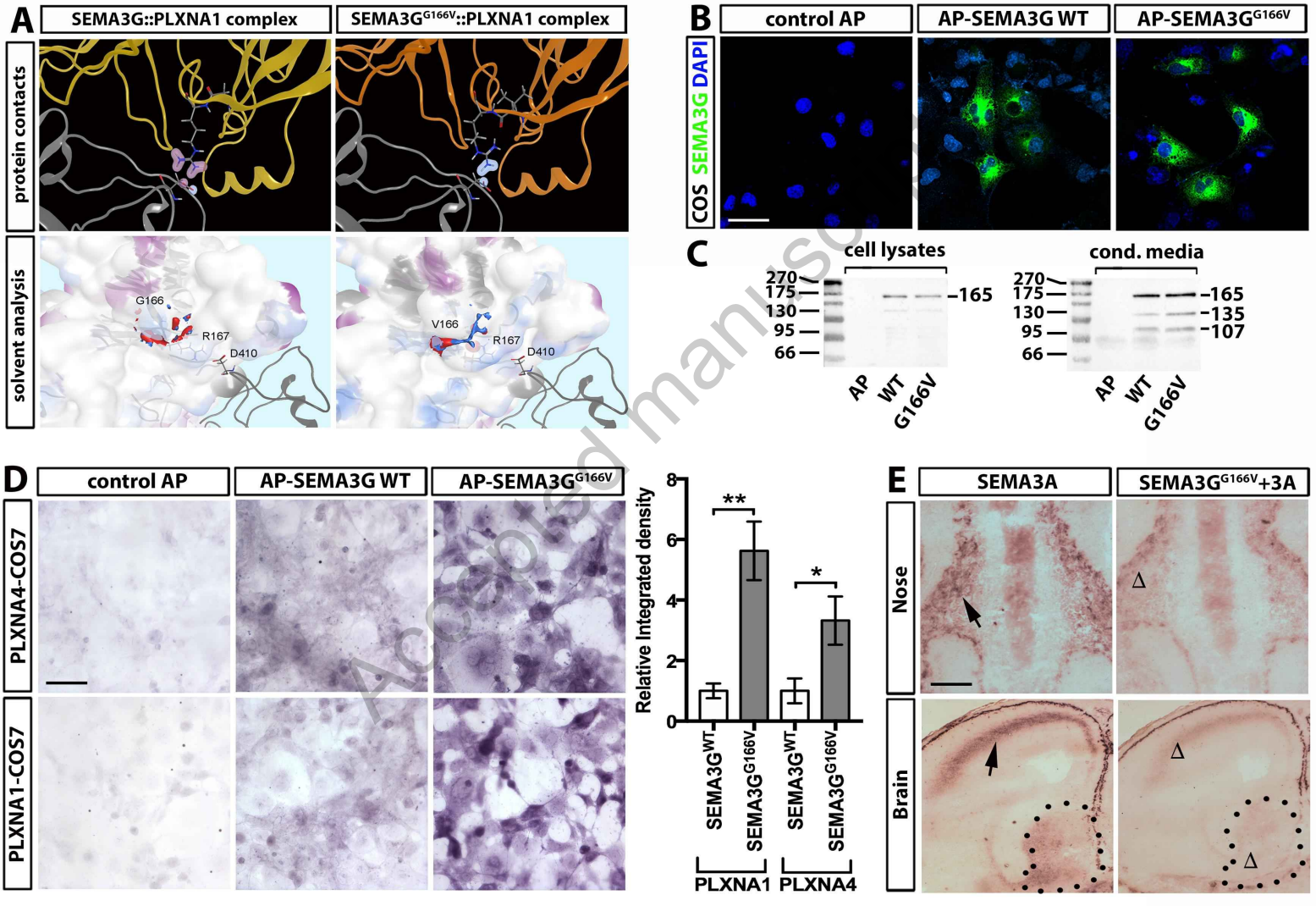

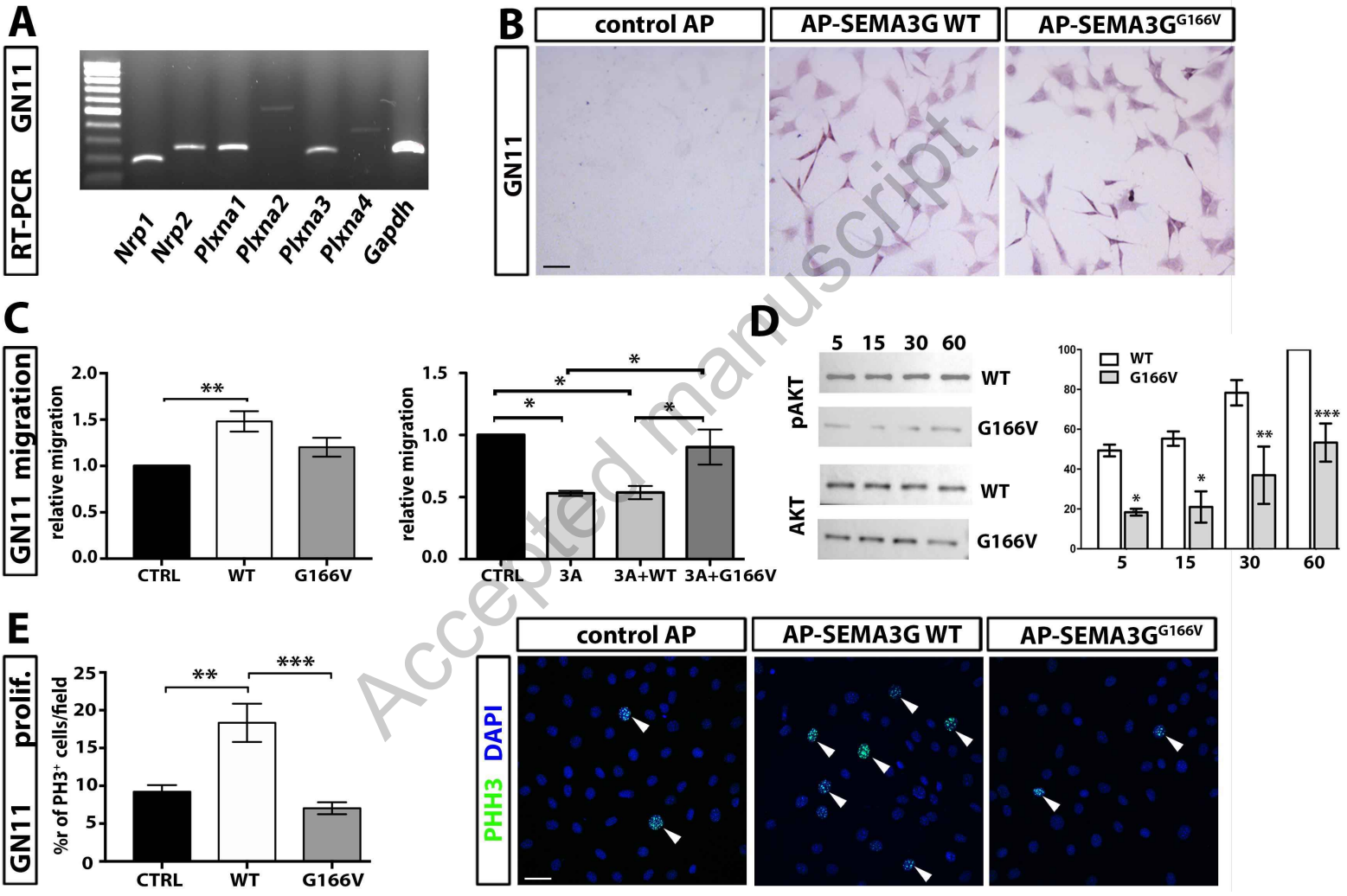

Supplementary figures and tables

Suppl. figure 1.

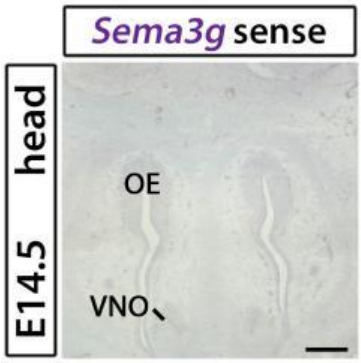

Suppl. Figure 1. Riboprobe for *Sema3g* is specific. ISH reactions on coronal E14.5 mouse sections at the level of the nose with sense probes *Sema3g* revealed absence of signal. Abbreviation: OE, olfactory epithelium; VNO, vomeronasal organ. Scale bar: 500 µm.

Suppl. figure 2.

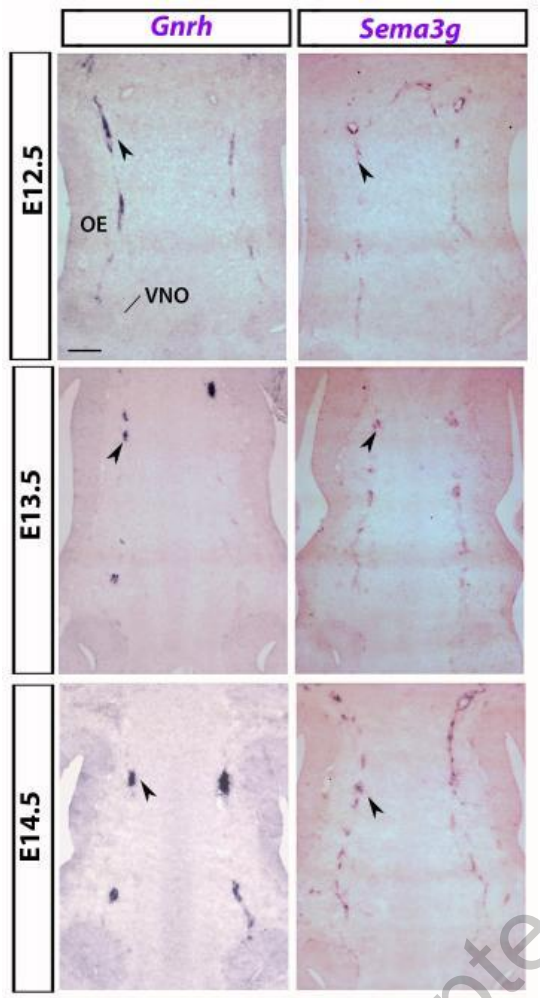

Suppl. figure 2. *Sema3g* mRNA expression during GnRH neuron development. Adjacent coronal sections of mouse heads at the indicated developmental stages were RNA-labelled for *GnRH* or *Sema3g*; black arrowheads indicate examples of migrating GnRH neurons and of Sema3g^{+} cells.

Suppl. figure 3.

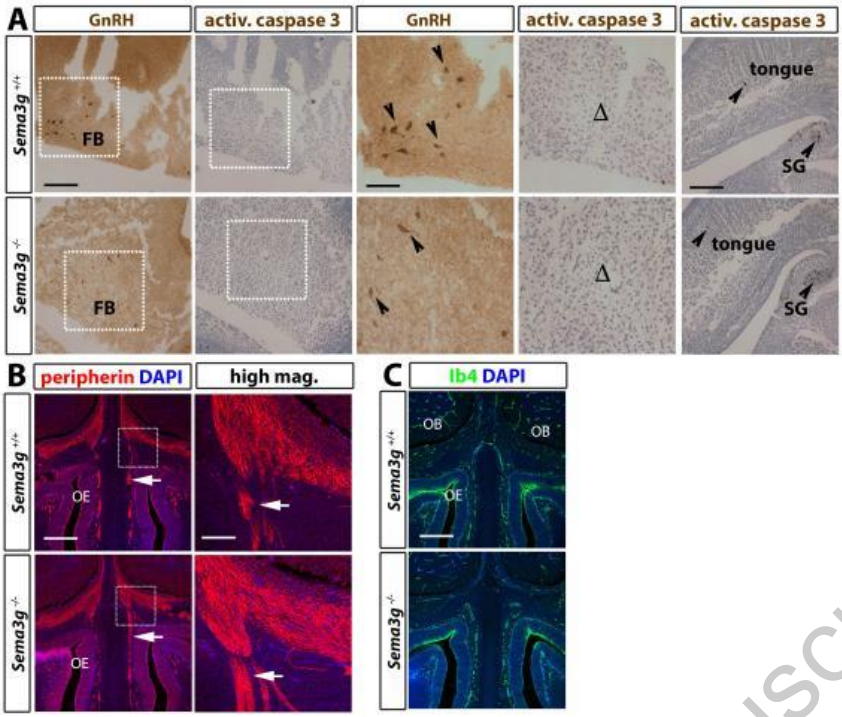

Suppl. figure 3. Forebrain cell death via apoptosis, nasal axonal and vascular patterning are not affected in the Sema3g-null embryos.

(**A**) Adjacent sagittal sections of E14.5 mouse heads of the indicated genotypes were immunolabelled for GnRH or activated caspase-3 to reveal GnRH neurons and apoptotic cells, respectively. High magnification areas indicated with white boxes are shown alongside. Black arrowheads indicate examples of GnRH neurons, while lack of apoptotic cells in the FB of wild-types and mutants is indicated with Δ. As positive control, sagittal sections of wild-type and *Sema3g*-null embryo heads at E14.5 were immunolabelled for activated caspase 3 to reveal apoptotic cells at the level of the tongue and of the salivary glands (SG) (right panels).
(**B-C**) Normal nasal axon and blood vessel patterning in *Sema3g*-null mutants. Coronal sections of E14.5 mouse heads of the indicated genotypes at the level of the nose were labelled with the blood vessel marker IB4 (**B**) or immunolabelled for peripherin (**C**). Nuclei were counterstained with DAPI. White arrowheads indicate examples of normal axonal branches projecting to the OB. Abbreviations: OB, olfactory bulb; OE, olfactory epithelium. Scale bars: 200 µm (**A**, low magnification), 100 µm (**A**, high magnification)
150 µm (**B–C**), 50 µm (higher-magnification images of boxed areas in **C**).

Suppl. figure 4.

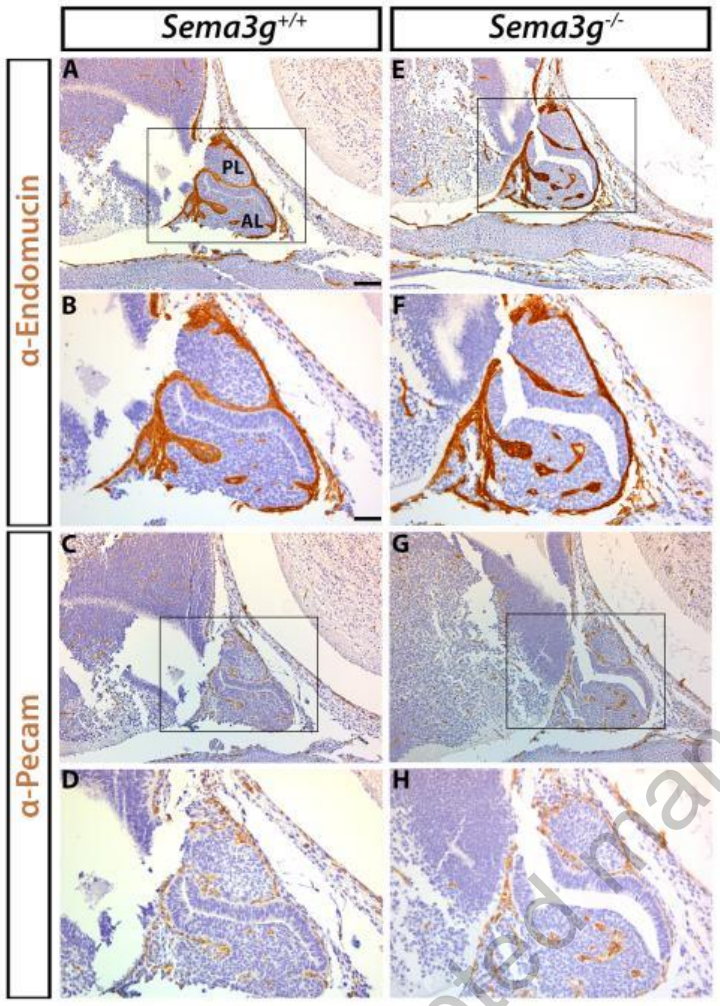

Suppl. figure 4. Pituitary vascular structure is not affected in the absence of *Sema3g.* Immunohistochemical analysis with vasculature markers Endomucin and Pecam on sagittal sections of control (**A-D**) and *Sema3g*$^{-/-}$ (**E-H**) mouse E14.5 embryos. (**B**) and (**F**) are the enlarged images of the boxed areas in (**A**) and (**E**), whereas (**D**) and (**H**) are the magnified images of (**C**) and (**G**), respectively. Embryos lacking *Sema3g* gene (**E-H**) show no abnormalities in the vascular architecture of the pituitary gland when compared to the stage-matched controls (**A**-**D**). Abbreviations: AL, anterior lobe; PL, posterior lobe. Scale bars: 200 µm (**A,C,E,G**), 100 µm (**B,D,F,H**).

Suppl. figure 5.

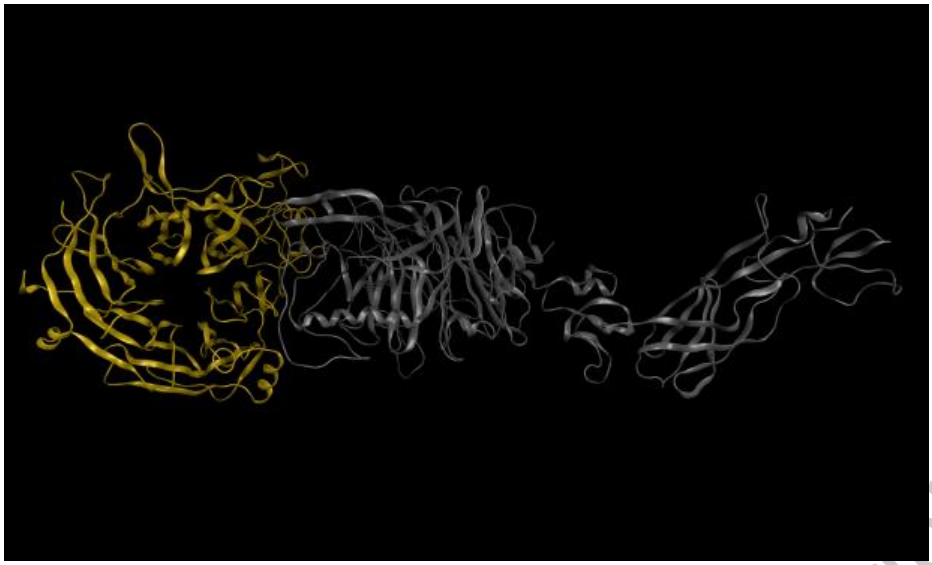

Suppl. figure 5. Homology model of SEMA3G::PLXNA1 complex.
The three-dimensional structures of human SEMA3G and PLXNA1 in complex are represented as yellow and grey ribbons, respectively.

Suppl. Table 1. Protein contact analysis of the wild-type and mutated SEMA3G; the energetic contribution of each single bond type to the interaction energy is reported.

PLXNA1	SEMA3G	Energy contribution SEMA3G WT (kcal/mol)	Energy contribution SEMA3G G166V (kcal/mol)	Interaction type
Asp410	Lys108	-1,597	-1,399	ionic
Asp410	Arg167	-6,575	-2,343	ionic
Asp410	Arg167	-1,722	-	ionic
Asp410	Arg167	-6,200	-	hbond
Leu389	Arg198	-5,000	-5,500	hbond
Lys391	Arg198	-3,400	-9,000	hbond
Glu223	Ala211	-4,900	-5,300	hbond
Asp234	Asp217	-2,700	-4,200	hbond
Asp234	Gln218	-6,400	-6,100	hbond
Asp234	Gln218	-6,200	-6,400	hbond
Lys391	Asp223	-7,354	-7,332	ionic
Lys391	Asp223	-8,900	-8,900	hbond
Lys238	Asp255	-7,170	-6,934	ionic
Lys238	Asp255	-	-1,185	ionic
Lys238	Asp255	-13,600	-15,200	hbond
Lys156	Gln277	-3,900	-0.900	hbond
Lys156	Gln277	-3,200	-10,600	hbond
Tyr96	Arg278	-3,200	-3,500	hbond
Tyr96	Arg278	-5,500	-5,800	hbond
Tyr197	Arg278	-0.600	-	hbond
Glu223	Asn282	-7,200	-7,100	hbond
Glu196	Arg409	-9,400	-9,100	hbond
Glu196	Arg409	-4,600	-0.800	hbond
Glu196	Arg409	-	-4,600	hbond
Glu196	Arg409	-6,577	-6,225	ionic
Glu196	Arg409	-3,469	-4,327	ionic
Glu196	Arg409	-1,998	-1,367	ionic
Glu196	Arg409	-6,563	-6,844	ionic
TOTAL		-137,325	-139,256	